Highly Dispersible Nanoparticle $BaTiO_3$ Synthesis and Dispersion Mechanism

(高分散性ナノチタン酸バリウムの合成とその分散メカニズム)

2018 年

李　金輝

Contents

1. Introduction

1.1 Properties of $BaTiO_3$

$BaTiO_3$ (BT) has been more than 70 years since it was found by America's Wainer and salomon[1], Japan's Ogawa[2], and Soveit's Wul and Goldman[3] in the early1940s. BT was confirmed as a member of the perovskite by Helen D. Megaw, Miyake, and Ueda [4.5]. It is well known that the formula for perovskite oxide is ABO_3, Barium is A side and Titanium is B side. The BT is cubic structure above Curie temperature of 120 ºC as Fig. 1-1 showing. Ba is located at each apex of cubic, Ti is located in the body center of cubic, and the oxygen is arranged on the each face center of cubic. BT is paraelectric for TiO_6 is symmetrical octahedron. In room temperature Ti slightly shifts to O in C axis direction, TiO_6 becomes asymmetrical and led to form a spontaneous polarization in BT crystal. The spontaneous polarization of BT can be inverted by an external electric field, makes BT appear ferroelectric. The structure of BT is very important that directly relates to its dielectric, piezoelectric and optical properties.

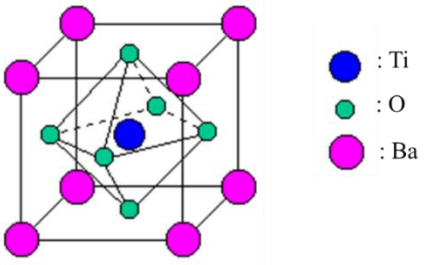

Fig.1.1-1 Structure of $BaTiO_3$

$BaTiO_3$ is widely applied in capacitor owing to its high dielectric constants and low dielectric loss. It has been reported [6, 7] that the dielectric constant is dependent on

temperature for its phase changes with temperature from rhombohedral, Orthorhombic, tetragonal, to cubic, although the relative dielectric constants are 1000 and 2000 in -80 and 0 ºC respectively, but the highest value of dielectric constants 6000-10000 is observed at Curie temperature 120 ºC which the crystal phase transforms from tetragonal to cubic. The characteristic is widely used in electronic devices, mainly multilayered ceramic capacitors (MLCCs). As the current market requires device miniaturization, larger capacity, and high performance, the dielectric layer constituting MLCCs must be thinner than 0.5 μm. The smallest MLCC of 0.25×0.125 has been already on sale by Murata Co. Ltd, replacing the 0402 (0.4 mm × 0.2 mm) that used in mobile phone.

1.2 Synthesis method of nanoparticle $BaTiO_3$

In this situation BT as the raw material of MLCC is also required to reduce the particle size to nanoscale. The synthesis of nanoparticle BT is mainly solid state and wet-state method. The solid state method is traditional synthesis of BT that the raw materials of $BaCO_3$ or BaO and TiO_2 have to be sintered at high temperature around 1000 ºC after ball milling [8-11]. The particle size BT obtained by this method is large around 3 μm, high aggregation and purity is low. These shortcoming lead to a reduction of BT electrical property. It is thought that the solid-state method is not suitable for the synthesis of

nanomaterial, for its inherent problem of high reaction temperature and heterogeneous solid phase reaction. Compering with solid state method the wet-state method can overcome these problems. It can control the chemical stoichiometry and obtain high purity, ultrafine BT. The method includes many approaches such as co-precipitation [12-14], low temperature directly synthesis (LTDS) under atmosphere [15], hydrothermal (HT) [16], sol-gel method [17], and so on. The LTDS and HT were studied here.

LTDS has been reported by Wada et al [15] that a 10-20 nm BT nanoparticle can be obtained from titanium tetrachloride ($TiCl_4$), barium hydroxide ($Ba(OH)_2$) and potassium hydroxide (KOH) in aqueous solution, as the reaction temperature above 50 ºC under atmosphere. The synthesis method is the simplest, and the cheapest in the BT nanoparticles, and suitable for mass production. But the particle size distribution is wide, aggregation among the particles is strong, and cubic phase is limited.

It is well known that the BT properties of ferroelectric, piezoelectric and nonlinear optical effect are all due to tetragonal structure. But as the particle size reduce to nanoscale, the two phase of tetragonal and cubic are mixed in a particle for their high surface energy. Hoshina et al [18] proposes that the nanoparticle BT have a core-shell structure, there is gradient lattice strain layer (GLSL) between inner tetragonal core and surface cubic layer. The surface cubic layer is about 10-15 nm does not change with particle size. It indicates

that the particle size depend on the inner tetragonal, and GLSL layer. These results was investigated by their XRD data. At the same time, there is critical size for the BT nanoparticle that BT is cubic crystal under a certain size. The critical size varies around 20 nm depending on the synthetic method [19. 20]. The core-shell structure is expected to have a high dielectric property.

The HT synthesis method is to synthesize the crystal material in high temperature aqueous solution under high a vapor pressure. The material dissolution, synthesis and growth of crystal can be accelerated in this condition. It is attracting attention in synthesis nanoparticle of ceramic material for the morphology, composition and size distribution of particle could be controlled simply in low reaction temperature. BT nanoparticle is also use this method, and the nanoparticle phase of BT can be controlled with raw material, reaction temperature and time and so on. But the drawback of this method is that the OH group from aqueous solution enter BT crystal, causes the defect of crystal and degrade the performance of the dielectric [21]. In order to avoid this disadvantage, several present of organic solvent is mixed to suppress OH defect [22].

1.3 Dispersion of nanoparticle

Nanoparticles are those having a particles size from 1 to 100 nm. It is different from

conventional bulk materials in properties of morphological [23], structural [24], thermal [25], electromagnetic [26, 27], optical [28, 29], mechanical [30] and so on. These properties due to its high surface activity and large surface area. Recently the nanomaterial is widely used in the different fields, such as, miniaturized electronic device, cosmetic, medical supplies, catalysts, pigments, toner and ink. However the aggregation property of nanomaterial affect the performance of the product. The properties of nanomaterial are not fully exploited. The high dispersion of nanoparticle is required.

As B. Faure et al [31] propose that the dispersion of nanoparticle have three approaches of electrostatic stabilization, steric stabilization, and electro-steric stabilization. It is well know that the electrostatic stabilization bases on DLVO theory. The DLVO theory was carried out by Derjagin and Landau of the old Soviet Union, and Verwey and Overbeek of the Nederland. The dispersion and aggregation of nanoparticle in aqueous suspension are well explained by the theory. There is two force existing between particles, one is electrical repulsion via the electric double layer, the other is the attractive force of van der waals. It is the basic theory to decide the dispersion or aggregation of particles in suspension solution via adjusting electrical repulsion force through controlling the amount of particle surface charge. E. Verwey et al [32] calculated the surface potential according to DLVO theory. It demonstrates that the 64.9 mV surface potential is necessary

to disperse 300 nm particle, and for the 20 nm particles 177 mV potential is necessary. In fact to disperser 20 nm particle in aqueous solution at same time the particle distance is under 5nm that calculated by the Woodcock formula (1) [33] shows in below, h is distance of particle surface, and F is the concentration of suspension. The concentration of the 20 nm particle suspension is not more than 10 vol% as it is mono-dispersion state. Actually, it is difficult to give high charge to the particle surface, and even if it is provided, the concentration of the solution is too low and the practicality is low. This is the limit of the DLVO theory.

$$h = d_p \left\{ \sqrt{\left(\frac{1}{3\pi F} + \frac{5}{6}\right)} - 1 \right\}$$

In addition to DLVO theory, recently the dispersion of ceramic nanomaterial has received much attention via the steric hindrance and electro-steric of polymer dispersant and Polyelectrolyte. The polymer thick layer adsorbs on the particle surface, blocks contact between particles, and prevent the aggregation of particles via the steric repulse from the long polymer chain.

PVP is synthesized from acetylene, ammonia, and formaldehyde. The monomer N-vinyl-2-pyrrolinde is carcinogenic but the polymer of PVP is a non-toxic [34], non-ionic [35] polymer with amphiphilic [36] for having C=O, C-N and CH_2 functional group. PVP dissolves well in aqueous and non-aqueous solution. It is widely used in cosmetic,

pharmaceuticals, food and so on. It is also used in ceramic material as dispersant [37], shape-control agent [38], and reductant agent [39].

1.4 Purpose of the study

We focused on the properties of dispersant PVP and practicality of BT. The purpose of the study is synthesis of highly dispersible nanoparticle of BT in one step, clarify the mechanism of nanoparticle forming and dispersion and obtains desired BT powder to satisfy the market requirement.

1.5 References

[1] E. Wainer and N Salomon, National Lead Co. Reports No. 8, 9, 10 (1938-1943)

[2] Ogawa, *J. Phys. Soc. Jnp.*, 1 [1]32-33(1946)

[3] B. M. Wul, and I. M. Goldman, Dokl. Akad. SSSR, 46, 154(1945) (in Russian).

[4] H.D. Megaw, *Nature* 155 484 (1945).

[5] S. Miyake and R. Ueda, *J. Phys. Soc. Jpn*. 1946, 1, 32.

[6] "Treasury of perovskite related compound functions" Edited by The Chemical Society of Japan (1997)

[7] Kiyoshi Okazaki "Ceramic dielectric engineering" Lecture donation company

(1969)

[8] M. Boulos, S. Guillement-Fritsch, F. Mathieu, B. Durand, T. Lebey, V. Bley, *Solid State Ionics* 2005, 176, 1301.

[9] H.S. Potdar, S.B. Deshpande, S.K. Date, *Mater. Chem. Phys*. 1999, 58, 121.

[10] L. Simon-Seveyrat, A. Hajjaji, Y. Emziane, B. Guiffard, D. Guyomar, *Ceram. Int*. 2007, 33,35.

[11] H. Xu, L. Gao, *J. Am. Ceram. Soc.*, 2003, 86, 203.

[12] A.V. Prasadarao, M. Suresh, and S. Komarneni, *Matter. Lett.* 1999, 39, 359.

[13] H. I. Hsiang and F. S. Yen, *J. Am. Ceram. Soc*, 1996, 79, 1053.

[14] F. S. Yen, H. I. Hsiang, and Y. H. Chang, *Jpn. J. Appl. Phys*, 1995, 34, 6149.

[15] S. Wada, T. Tsurumi, H. Chikamori, T. Noma, T. Suzuki, *J. Crystal. Growth* 2001, 229, 433–439

[16] K. Kiss, J. Magder, M. S. Vukasovich, and R. J. Lockhart, *J. Am. Ceram. Soc*, 1996, 49, 291.

[17] M. H. Frey and D. A. Payne, *Phys. Rev. B.* 1996, 54, 3158.

[18] T. Hoshina, S. Wada, Y. Kuroiwa and T. Tsurumi, *Appl. Phys. Lett.* 2008, 93 192914

[19] S. Schlag and H. –F. Eicke, *Solid State Comm.* 1994, 91 (11]), 883-887

[20] Y. Hakuta, H. Ura, H. Hayashi and K. Arai, *Ind. Eng. Chem. Res.* 2005, 44, 840-846.

[21] J. Adam, G. Klein and T. Lehnert, *J. Am. Ceram. Soc.*, 2013, 96, 2987-2993.

[22] Kwon, B. Park, K. Choi, E. Choi, S. Nam, J. Kim, J. Kim, *J. Eur. Ceram. Soc.*, 2006, 26, 1401-1404.

[23] H. Maeda: *J. Control. Release*, 1992, 19, 315–324.

[24] H. Suzuki, T. Ohno: *J. Soc. Powder Technol. Jpn*, 2002, 39, 877–884.

[25] N. Wada, *Chem. Eng.*, 1984, 9, 17–21.

[26] K. Ishikawa, K. Yoshikawa and N. Okada, *Phys. Rev. B,* 1988, 37, 5852–5855.

[27] M. Haruta, *Catalysts*, 1994, 36 (6) 310–318.

[28] Y. Kurokawa, Y. Hosoya: *Surface*, 1996, 34 (2) 100–106.

[29] K. Kobayashi, *J. Soc. Powder Technol., Jpn*, 2004, 41, 473–478.

[30] K. Niihara, *J. Ceram. Soc. Jpn*, 1991, 99(10), 974–982.

[31] Bertrand Faure, German Salazar-Alvarez1, Anwar Ahniyaz, Irune Villaluenga, Gemma Berriozabal, Yolanda R De Miguel and Lennart Bergström, Sci. Technol. *Adv. Mater.* 14 (2013) 023001 (23pp)

[32] E. Verwey and J. Th. G. Overbeek : “Theory of the Stability of Lyophobic Colloids”, Elsevier, Amsterdam, Netherlands, (1948).

[33] L.V. Woodcock, Proceeding of a workshop held at Zentrum fur interdisziplinare Forschung University Bielefield, Nov. 11-13, 1985 Edited by Th. Dorfmuller and G.Williams. CNingthoujam, A. B. Salunkhe and S. H. Pawar, *New J. Chem.*, 2013, 37, 3121.

[35] G. Lu, S. Li, Z. Guo, O. K. Farha, B. G. Hauser, X. Qi, Y. Wang, X. Wang, S. Han, X. Liu, J. S. DuChene, H. Zhang, Q. Zhang, X. Chen, J. Ma, S. C. J. Loo, W. D. Wei, Y. Yang, J. T. Hupp and F. Huo, *Nat. Chem.*, 2012, 4, 310.

[36] Synthesis of Noble Metal Nanoparticles Ph.D. Thesis, ed. M. Bahadory, Drexler University, USA, 2008.

[37] R. Si, Y.-W. Zhang, L.-P. You and C.-H. Yan, *J. Phys. Chem. B*, 2006, 110, 5994.

[38] X. Wu, Y. Zhao, C. Yang and G. He, *J. Mater. Sci.*, 2015, 50, 4250.

[39] Y. Xiong, H. Cai, B. J. Wiley, J. Wang, M. J. Kim and Y. Xia, *J. Am. Chem. Soc.*, 2007, 129, 3665.

2. High dispersion cubic $BaTiO_3$ synthesis and evaluation

2.1 Introduction

As the chapter.1 described, barium titanate (BT, $BaTiO_3$) is an important ceramic material for its ferroelectric, dielectric and thermoelectric [1]. It is well known that it is mainly used in multilayered ceramic capacitors, semiconductors, positive temperature coefficient (PTC) thermistors, and piezoelectric devices [2–7]. In recent years the BT nanoparticle size with spherical shape is required along with the device miniaturization. Because the high sintering density can be obtained in low sintering temperature and a low dissipation factor can be obtained in high dielectric constant.

At present, the BT nanoparticle can be prepared simply by wet chemical process, such as sol-gel method [8], hydrothermal [9], low temperature synthesis at atmosphere [10] and so on. But the problem is aggregation with BT particle size (PS) decreasing which reduces the performance of the electronic components. It is very important to prevent the particles aggregation.

There are three kinds of dispersion approaches of nanoparticle: (1) Dispersant is directly put into the nanoparticle suspension [11-13]. (2) Dispersant react to the nanoparticle that its surface is pretreated by hydroxylation [14]. These methods are

required two step, one is nanoparticle synthesis, the other is dispersion. Recently, it has been reported that the dispersant is directly added into reaction solution with the raw material for preparing nanoparticle [15−21]. The third method can be simply realize the syntheses and dispersion in a single step.

Hai et al., [22] has reported that high dispersion BT particle can be prepared with raw material and direct modification of PVP on the BT surface in a single step. The spherical 300 nm BT particles were obtained by $TiCl_4$, $BaCl_2$, and PVP in an aqueous solution which demonstrated mono-dispersion in aqueous solution. But the PS is still large as nanoparticle, and the dispersion of BT particle becomes worse with the PS decreasing in this process.

In order to obtain a spherical, high dispersion, and nanosize of BT particle, and clarify the mechanism of particle growth and dispersion in this original process, the reaction factors such as: temperature, time, concentration of raw material, PVP molecular weight were systematically investigated, and achieved desired PS of high dispersion BT by controlled this process parameters. XRD, FE-SEM, TEM, DLS, zeta-potential were used as the means of evaluation. The particles prepared by the low temperature synthesis (LTS) is referred LBT-PVP in this section.

2.2 Experiment

2.2.1 Materials

The precursors titanium tetrachloride ($TiCl_4$ 90+%), Dihydration barium chloride ($BaCl_2 \cdot 2H_2O$ 90%) and the mineral agent of Potassium hydroxide (KOH 85%) were purchased from Wako Pure Chemical Industries Ltd. Japan. The dispersant of polyvinylpyrrolidone (PVP) was bought from Sigma-Aldrich Wako Pure chemical Japan.

2.2.2 Synthesis of LBT–PVP nanoparticle

The procedures of the LBT–PVP preparation process and characterization are shown in Fig. 2.2-1. The concentrations of KOH, PVP and the raw materials (Ti and Ba sources), molecular weight of PVP as well as the reaction temperature and reaction time were varied; the values of these parameters are summarized in Table. 2.2-1.The pH of the solution was over 14, for the KOH concentration was higher than 1.6 M in this study. As the Fig. 2.2-1 showing, the Ba and Ti sources: $BaCl_2 \cdot H_2O$, $TiCl_4$ were mixed in reaction container. PVP was simultaneously added to the mixture while stirring. After PVP was completely dissolved in the mixed solution, KOH was slowly drop wised. Finally, the mixed solution (80 mL) was set to desire temperature and time. After cooling, solid precipitates were obtained by centrifugation. The precipitates were washed with distilled water and ethanol, and dried at 60 °C for 24 h.

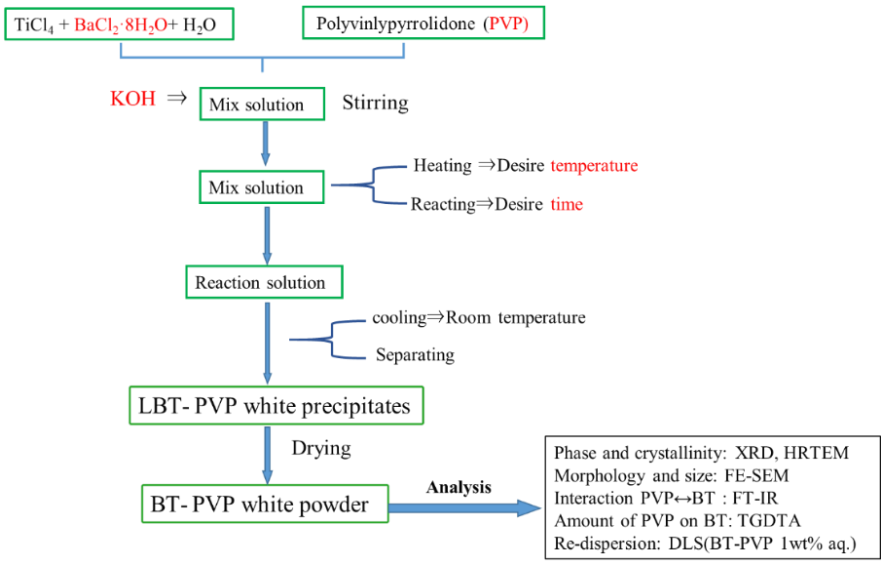

Fig. 2.2-1 Flow chart of preparation and analysis of LBT–PVP

Table. 2.2-1 Reaction factor of synthesis LBT-PVP in section 2. The standard reaction condition is that Ti:Ba = 0.2M:0.2M, KOH = 1.8 M, PVP = 100 g/L, 80 ºC, 60 min

Factor	
Temperature (ºC)	75, 80,85, 90
Time (min)	0, 30, 60, 90, 120, 150, 180, 210, 240
Ba conc.(M)	0.2, 0.3, 0.4
KOH conc.(M)	1.6, 1.7, 1.75, 1.77, 1.8, 1.81, 1.84, 1.9, 2.3, 2.5
PVP conc.(M)	0, 50, 100, 350, 400, 450
PVP Mw (g/mol)	2500, 10000, 40000, 360000

2.2.3 Characterization

The phase of the powder was investigated by X-ray diffraction (XRD; Smartlab, Rigaku Corp., Japan). The morphology of the BT particle was observed by field-emission scanning electron microscopy (FE-SEM; JSM-6335M, JEOL Ltd., Japan). Transmission electron microscopy (TEM), high-resolution TEM (HRTEM), images and corresponding

fast Fourier transform (FFT) pattern were carried out at accelerating voltage of 200KV by US70, Hitachi Ltd., Japan. The PS and size distribution of the dry powder were determined by analyzing the FE-SEM images with the specialized software SMileView (JEOL, Japan). The dispersion of the powder in aqueous solution was evaluated by Dynamic light scattering (DLS; FPAR-10001, Otsuka Electronics Co., Ltd., Japan) with aqueous suspension of 1 wt% LBT–PVP. The dispersion state of LBT-PVPs in aqueous was directly observed by FE-SEM with a Trans-SEM of sample holder. The sample suspension was drop into the chamber in the TransSEM holder between two silicon nitride films. As the reported by Izu et al., [23] a 3 μL 1 wt.% BT–PV aqueous suspension was dropped into the chamber, and set in the SEM to be scanned by a secondary electron detector. Thermogravimetric analysis (TGA; TG-DTA2010SA. Bruker AXS K.K., Germany) was used to evaluate the amount of PVP adsorbed on the surface BT. The chemical bonding of the PVP dispersant on the surface of BT was identified by Fourier-transform infrared (FT-IR) spectrometry (FT/IR-610, JASCO, Japan). The zeta-potential of LBT-PVPs were evaluated by ELS-Z1/Z2 (Ostuka Electronics Co., Ltd., Japan).

2.3 Results

2.3. 1 Effects of reaction temperature and reaction time

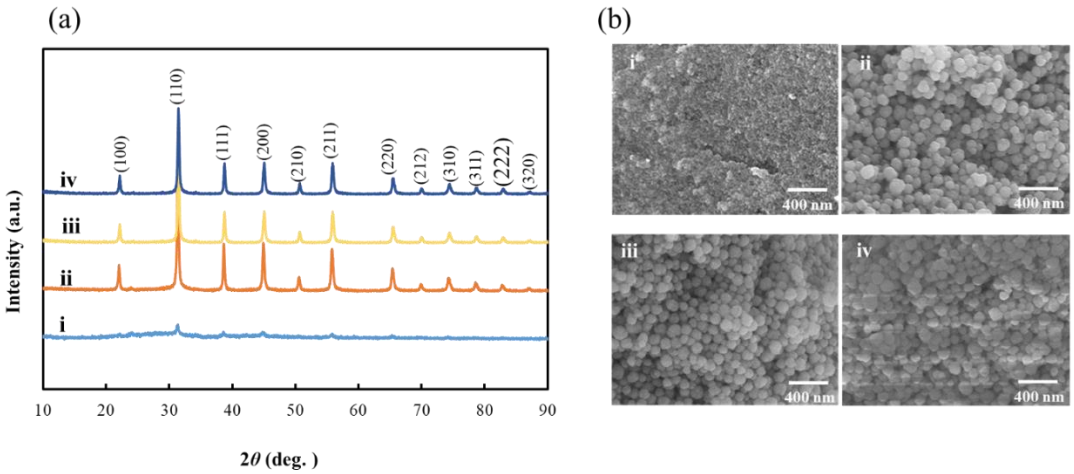

Fig. 2.3-1 XRD (a) and FE-SEM image (b) of LBT–PVP prepared in different temperature. (i) 75°C, (ii) 80°C, (iii) 85°C, (iv) 90°C

The effect of temperature on LBT–PVP synthesis was investigated. The concentration of precursors Ti and Ba were 0.2M respectively, the mineral KOH was 1.8M, and the dispersant PVP was 100 g/L. The samples were collected as the reaction solution temperature reached to 75, 80, 85, and 90 °C. Fig.2.3 -1(a) shows XRD diffraction patterns of LBT–PVP collected in each temperatures of reaction solution. The weak peaks of BT collected at 75 ºC could be observed, indicating that LBT-PVP has begun to form. On the other hand, the peak of LBT–PVP collected in 80 °C, clearly observes with strong intensity, which is good agreement with the PDF card No: 79-2263, indicating that the phase of LBT–PVP collected at 80 °C is cubic, as Wada et al., [24] and Hai et al., [22] reported. The crystallite size of BT prepared at 75, 80, 85, and 90 °C was

20.9, 42.3, 39.7, and 39.7 nm, respectively calculated by Scherrer equation with the corresponding peak of (110) plane in XRD pattern. The crystallite size was twice times from 75-80 °C, but was not changed exceeded 80 °C. These indicates that the crystallite growth was so fast until 80 °C.

Fig. 2.3-1(b) is the FE-SEM image of the dried powder collected at 75–90 °C. The drying sample collected at 75 °C is a gel. Several 10-20 nm fine particles are buried in the gel. This agrees to XRD pattern, that the intensity of LBT–PVP peak is very weak in Fig. 2.3-1(a). The uniform spherical particles can be observed from 80 °C, and the PS was not change with increasing temperature.

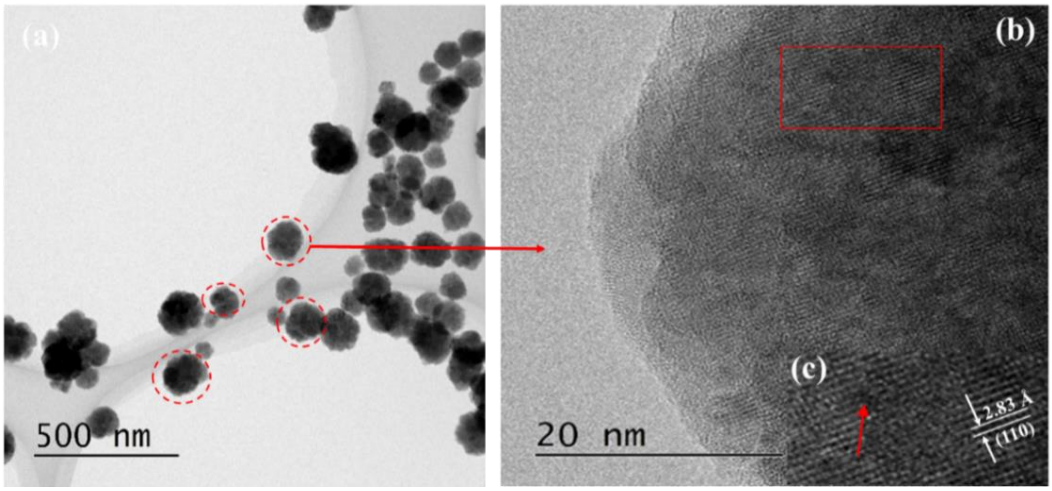

Fig. 2.3-2(a) TEM image of LBT–PVP prepared at 80 ºC. (b) HRTEM image (c) An enlarged HRTEM image of the square surrounded by red line.

In order to directly to observe the particle crystallinity, the LBT–PVP prepared with PVP 100g/L in 80 °C was selected to be observed by TEM. The image of TEM shows in Fig. 2.3-2(a). It can be seen that the spherical particle consists with several crystals separated by grain boundary as red dashed line surrounded. Figure. 2.3-2 (b) shows the HRTEM image of the particle surrounded by red dashed line in Figure. 2.3-2 (a). The lattice fringes can be observed, but is not continuous. The interval of lattice fringe is 0.283 nm, which agree with the spacing of the (110) planes of the cubic BT structure in the Fig. 2.3-2 (c) that the enlarged image of the square surrounded by red lines in Fig. 2.3. 2 (b). These results indicate that the particle of LBT-PVP is cubic polycrystalline.

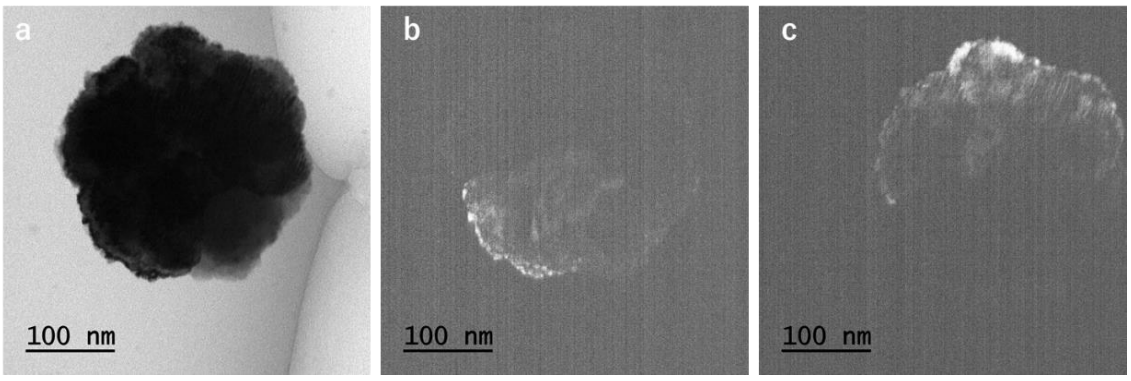

Fig. 2.3-3(a) TEM Image of LBT-PVPs prepared in 90℃for 2h. (b) and (c) are TEM images of (a) observation in

The particle (Fig. 2.3-3(a)) was observed in restricting the field of view with the

restricted visual field diaphragm as a whole, the alignment of two periodic diffraction points was confirmed. Each one of diffraction points with a periodicity was observed in dark field, Fig. 2.3-3(b) and (c) show the images. These results indicate that the particle is consisted with several single crystals in different orientation via aggregation of single crystals. It also proves that the particle of BT prepared in low temperature under atmosphere is poly-crystal.

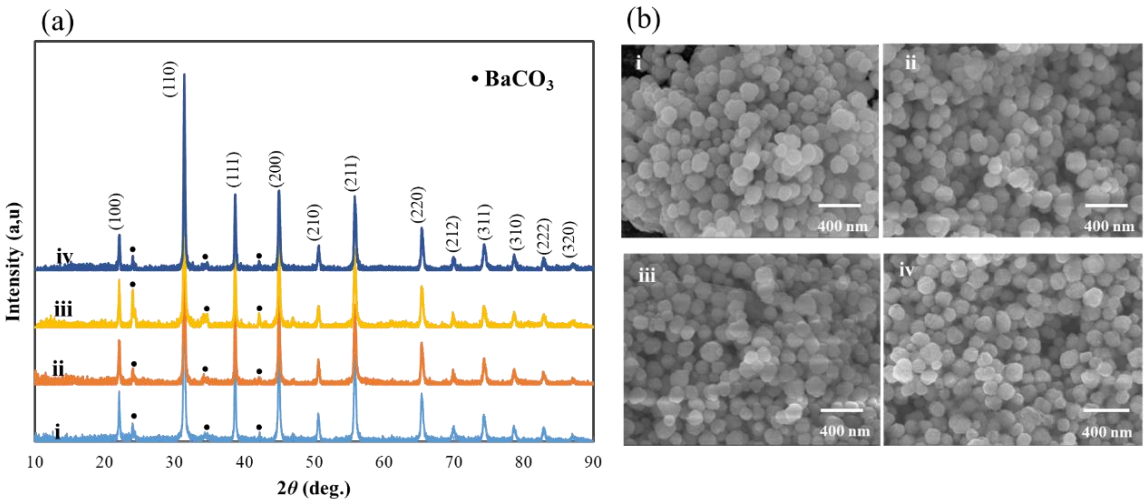

Fig. 2-3-4 XRD (a) and FE-SEM image (b) of LBT–PVP prepared in different reaction time. (i) 0 min, (ii) 60 min, (iii) 120 min, (iv)180 min

It can be concluded that the LBT–PVP particles could be prepared from 75 °C, and the PS is not change with temperature increasing above 80 °C based on the above results of temperature effect. Then the effect of reaction time on the particle growth was investigated at 80 °C. The samples were collected as the reaction time reached 0, 20, 40,

60, 90, 120, 150, 180, 210, and 240 min. Fig. 2.3-4(a) is the XRD diffraction patterns of these samples, which demonstrates that the phase of the samples is cubic, agreement to the result in Fig. 2.3-1(a) and proving that the cubic phase did not change with reaction time. It also can be observed that the peak intensity of $BaCO_3$ marked with black spots is stronger than the peak in Fig. 2.3-1.It indicates that $BaCO_3$ formation is unavoidable under CO_2-free in atmosphere and the amount of impurity $BaCO_3$ slightly increase with reaction time. Wada et al., [24] also reported that the purity $BaTiO_3$ could be synthesized in a N_2 atmosphere. The spherical particle could be observed in FE-SEM image as Fig 2.3-4(b) showing. The spherical particles were formed at 0 min (the start time), and their morphology and size did not change with increasing reaction time. It indicates that the progress of reaction was very fast for a raw material concentration of 0.2 M. T Fig.2.3.1-4 shows the relationship between the PS measured by the FE-SEM image and reaction time. The particles do not grow large with reaction time around 170 nm. It maybe that the PVP becomes thin layer absorbed on the BT surface, and prevents the further growth of BT particle.

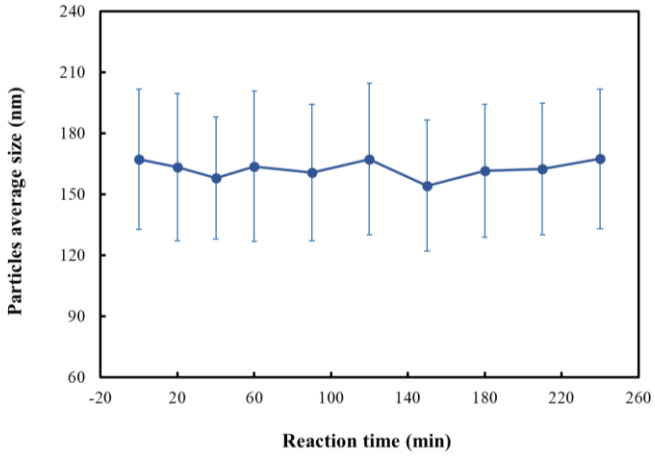

Fig.2.3-5 Relationship between PS of BT–PVP and reaction time.

2.3.2 Effect of Ba concentration

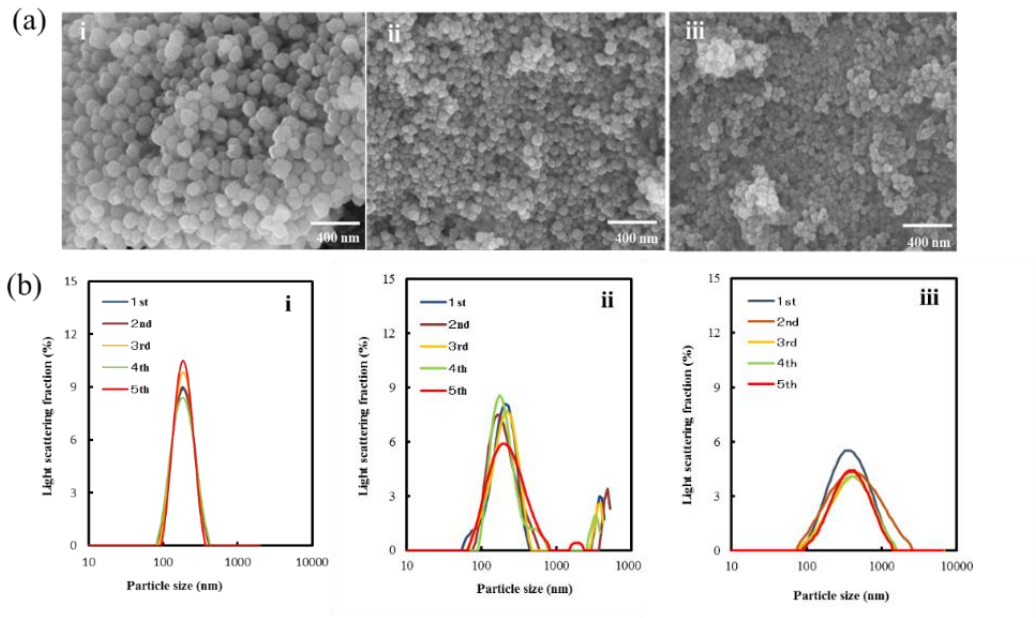

Fig. 2.3-6 (a) FE-SEM images and (b) DLS pattern of nanoparticle LBT–PVPs prepared in different concentration Ba^{2+}. The Ti^{4+} concentration is fixed at 0.2 M, and Ba^{2+} concentration is (i) 0.2 (ii) 0.3 and (iii) 0.4 M.

In our previous study, the PS of LBT–PVP was around 250 nm prepared at 0.1 M Ba and 0.1M Ti sources [22]. In order to reduce the PS, the raw material concentration of Ba and Ti were increased two times. In addition, the Ba concentration was adjusted to 0.2 and 0.4 M. Fig. 2.3-6 (a) is FE-SEM images of LBT−PVP powder prepared at different Ba concentrations. The PS of LBT−PVP decreased from 130, 62 to 52 nm with increasing Ba concentration from 0.2, 0.3, to 0.4 M respectively. As the classical nucleation and growth model that reported by Li and Shin [25] the driving forces for nucleation becomes stronger with increasing Ba concentration, the large amount of small nuclei were formed in reaction solution, then particles growth were restrained. The spherical and uniform morphology of the LBT–PVP nanoparticles were also observed in the FE–SEM images.

The dispersion of LBT–PVP nanoparticle was evaluated by PS measured by DLS with 1 wt% LBT–PVP aqueous suspension. Fig. 2.3-6 (b) shows the DLS pattern of LBT–PVPs prepared at different Ba concentration. The particles size increases from 175, 296 to 386 nm with the Ba concentration increasing. The PS distribution is the narrowest at a Ba concentration of 0.2M, and then becomes broad with increasing Ba concentration. The LBT-PVP particles prepared at 0.2M Ba in aqueous solution demonstrate mono-dispersion for the PS is close that measured by SEM and DLS respectively (130 nm measured by SEM, 175 nm measured DLS). But the LBT-PVPs particles prepared at 0.3,

0.4 M Ba in aqueous solution demonstrate strong aggregation from several particles for the PS measured by DLS are larger (296, 386 nm) than that one measured by FE–SEM (62, 52 nm). It concludes that the PS decreases and re-dispersion becomes poor with raw material concentration increasing.

2.3.3 Effect of KOH concentration

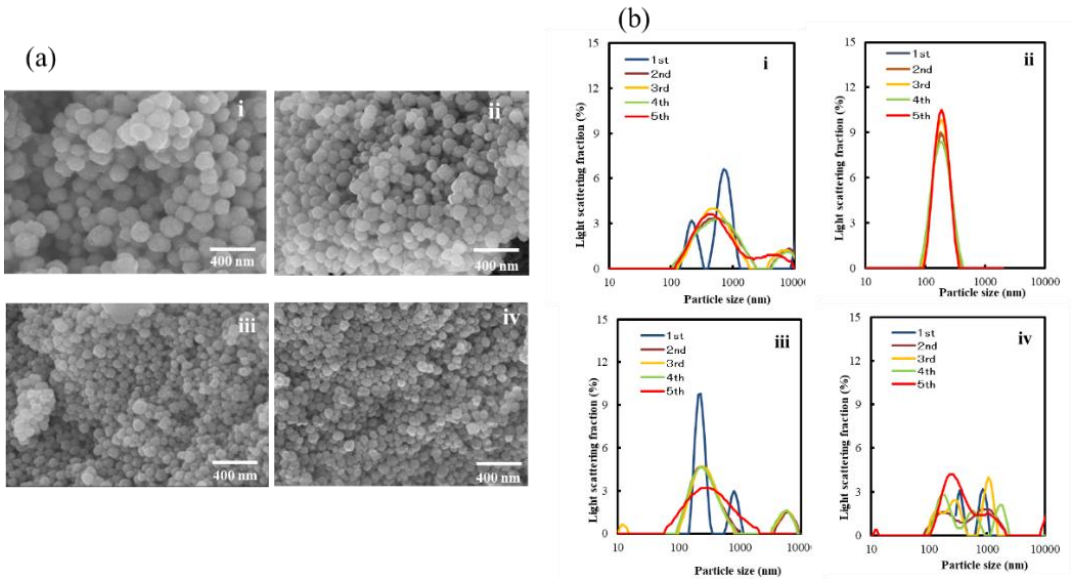

Fig. 2.3-7 (a) FE-SEM images and (b) DLS pattern of nanoparticle LBT–PVPs prepared in different KOH concentration. (i) 1.6, (ii) 1.8, (iii) 2.3, (iv) 2.5 M

Lee et al., [26] suggested that the mineral agent KOH affect the formation of $[Ti(OH)_4]^{4-x}$ and the chemical reaction of Ba^{2+} to $[Ti(OH)_4]^{4-x}$. So it is very important to investigate the effect KOH concentration on the PS, morphology, and dispersion in this study with PVP in reaction solution.

Fig. 2.3-7(a) shows FE-SEM images of nanoparticle LBT–PVPs prepared in different KOH concentration. The PS of LBT–PVPs decreased from 201, 130, 102 to 86 nm with KOH concentration increasing 1.6, 1.8, 2.3, 2.5 M. Fig. 2.3-7(b) shows DLS pattern of these nanoparticle LBT–PVPs in aqueous solution. It can be observed that only the LBT–PVP prepared at 1.8M KOH solution demonstrates high dispersion for the DLS patterns of five sequential measurements are almost same as. Although the PS (175 nm) measured by DLS slightly larger than that one (130 nm) measured by SEM, it was thought that the LBT–PVP demonstrated mono-dispersion in aqueous solution. Izu et al., [23] has reported the PS measured by DLS is calculated from the refractive index and viscosity of the dispersion solution, it is usually larger than that measured by SEM.

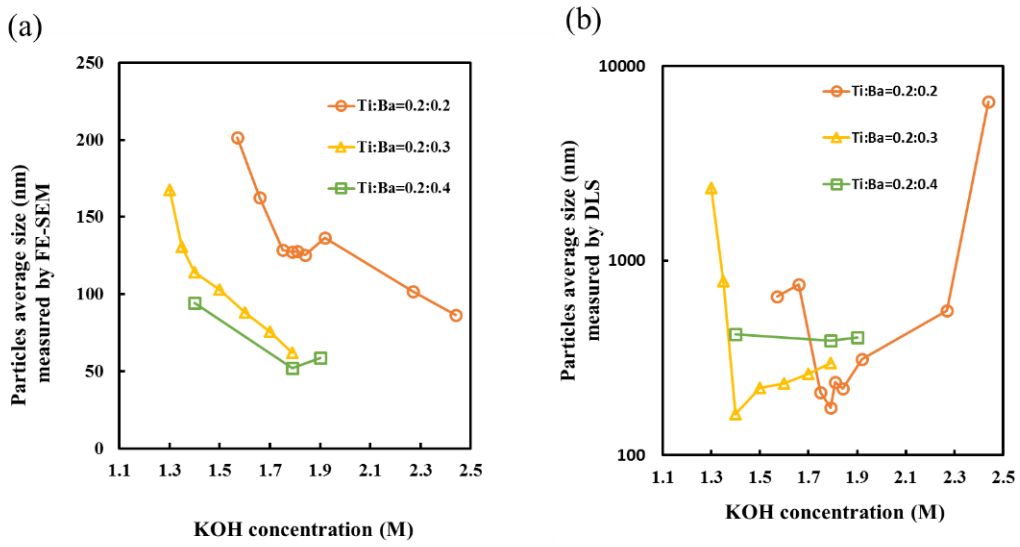

Fig. 2.3-8 Effect of KOH concentration on the PS of LBT–PVPs that measured by FE-SEM (**a**) and DLS (**b**) respectively. The LBT–PVPs prepared at material sources ratio of

Ti: Ba is 0.2: 0.2, 0.2: 0.3, and 0.2 M: 0.4 M respectively and the other condition is PVP =100 g/L 80 ºC, 1h

The relationship of KOH concentration and PS of LBT-PVP measured by FE-SEM (a) and DLS (b) shows in Fig. 2.3-8. The BT-PVPs were prepared for different mole ratios: [Ti]/[Ba] = 0.2 M:0.2 M, 0.2 M:0.3 M, and 0.2 M:0.4 M. The PS measured by FE-SEM decreased with the KOH and Ba concentration increasing as show in Fig. 2.3.3-2 (a). Lee et al., [26] and Newalkar et al., [27] also reported same tendency. As the section 2.3.2 discussed, it was though that high KOH concentration also accelerated the nucleation and crystal formation. The particle growth is suppressed for the large number of small crystals formation in reaction.

The relationship between the KOH concentration and LBT-PVP dispersion is shown in Fig. 2.3-8 (b). The dispersion is evaluated by the PS of LBT-PVP in aqueous solution measured by DLS. The PS is very small around 200nm that prepared at [Ti]/[Ba] ratio of 0.2 M:0.2 M under KOH concentration range from 1.7 to 1.9 M. The LBT-PVP particles show high dispersion that prepared in this range of KOH concentration comparing with the powder PS 150 nm as Fig. 2.3-8(a) showing. The range of KOH concentration is from 1.4 to 1.9 M for [Ti]/[Ba] ratios of 0.2 M:0.3 M and 0.2 M:0.4 M. The PS is 250, and 400 nm respectively. The particles show slight aggregation comparing with the powder's PS

under 100 nm as showing in Fig. 2.3-8 (a). This indicates that the aggregation of nanoparticles become strong with PS of powder decreasing, so the PS measured by DLS increases with Ba concentration increasing. There is optimum kOH concentration for mono-dispersion BT-PVP prepared at different source ratio of [Ti]/[Ba], such as the source ratio of [Ti]/[Ba] = 0.2 M:0.3 M showed at 1.4 M KOH, because the PS of 114 nm measured by FE-SEM is closed to that of 162 nm measured by DLS and for [Ti]/[Ba] = 0.2 M:0.2 M showed at 1.8 M KOH, because the PS of 130 nm measured by FE-SEM was closed to that of 175 nm measured by DLS.

2.3.4 Effect of PVP concentration

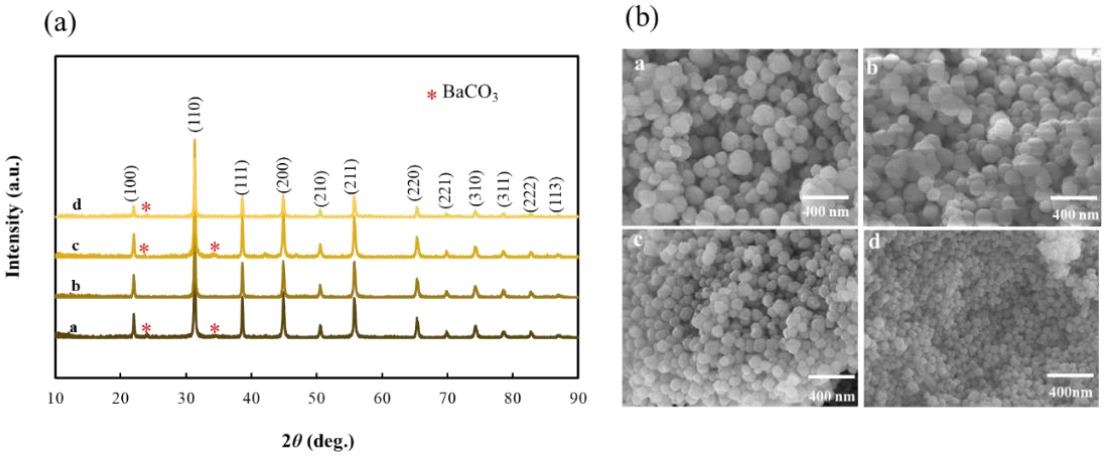

Fig.2.3-9 XRD diffraction pattern (a) and FE-SEM images (b) of LBT–PVPs prepared with different concentration PVP solution. (a) 0, (b) 25, (c) 100, and (d) 450 g/L.

It has been reported that the morphology, size, and dispersion of nanoparticles could

be adjusted in situ polymer-assisted particle growth [23, 28]. In our previous study, it has been reported that the effect of PVP concentration on the PS and dispersion of BT–PVP [22]. The results demonstrated that the PS decreased with PVP concentration increasing. But it was inadequate for the source concentration (0.1 M) was low, and PVP concentration range (60–200 g/L) was narrow. In this study the source concentration of Ba and Ti are doubled. It is well known that the PS will be small as the source concentration increasing. In order to disperse the small BT-PVP particles, the range of the PVP concentration had to be further broadened from 0 to 450 g/L. Fig 2.3-9(a) is the XRD pattern of BT–PVPs prepared by different PVP concentration. Their phases were cubic for good agreement to PDF card No: 01-79- 2263. The lattice parameter and crystallite size was calculated by Scherrer's Equation using the (110) plane peak in XRD pattern. The lattice parameter was 4.04 Å, indicating that it did not change with PVP concentration. However, the crystallite size decreased from 48.7 to 39.2 nm with the PVP concentration increasing from 0 to 300 g/L. On the contrary, as the PVP concentration further increased, the crystallite increased to 50.7 nm which was close to the size of BT–PVP prepared without PVP. It can be observed that the morphology of these BT–PVPs were spherical although PS were decreased from 205 to 97 nm with PVP concentration increasing as the Fig 2.3-9(b) showing. Table 2.3-1 summarize these results in detail.

Table 2.3-1 Calculation and measurement results of LBT–PVPs prepared in different PVP concentrations. The molecular weight of PVP was 10,000 g/mol.

Sample	PVP conc. (g/L)	Lattice parameter (Å)	Crystallite size[a] (nm)	PS[b] (nm)	Crystalline No. in a particle
Conc.1	0	4.0404	48.7	205	75
Conc.2	25	4.0401	49.0	191	59
Conc.3	50	4.0428	44.5	141	31
Conc.4	100	4.0408	43.3	130	27
Conc.5	200	4.0409	40.1	120	26
Conc.6	300	4.0405	39.2	102	18
Conc.7	350	4.0399	51.8	116	11
Conc.8	450	4.0423	50.7	97	7

[a] Calculated using Scherrer's equation.

[b] Measured by FE-SEM.

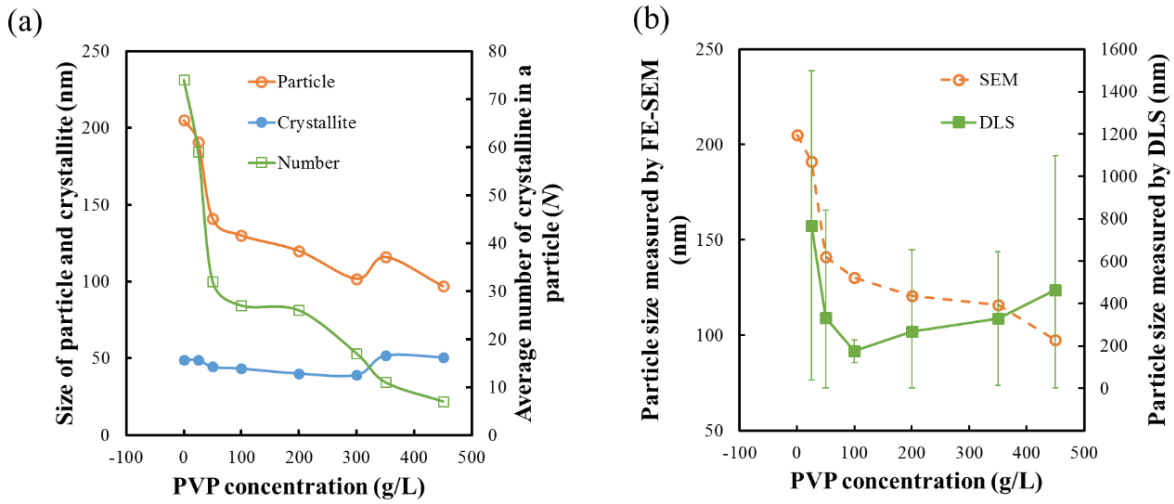

Fig. 2.3-10 (a) Effect of PVP concentration on PS, crystallite size, and average number of crystallite in a particle of LBT–PVP. (b) Effect of PVP concentration on the PS of LBT–PVPs measured by FE-SEM and DLS.

Fig. 2.3-10 (a) shows the effect of PVP concentration on PS, crystallite size, and average number of crystallite in a particle. The PS of LBT–PVPs decreased from 205 to 97 nm with increasing PVP concentration, indicating that the particle growth was inhabited by PVP. The numbers of crystallite in a particle was calculated by the spherical volume of a LBT–PVP divided by a crystallite volume (also regarded as sphere). The numbers of crystallite in a particle decreased with PVP concentration increasing. It indicates that the particle was consisted of several crystallites. It is well known that the crystallite growth is due to the strong attractive force among BT nucleus, the particle growth induces from the aggregation of several crystallites by relatively weak attractive force. It has been reported that the space among PVP network decreases with PVP concentration increasing [29]. The growth of particle and crystallite have to remove the interference from the PVP network, so the size of particle and crystallite became small with the PVP concentration increasing. It is possible that the particle growth was badly distributed in a high PVP concentration (such as 450 g/L), the crystallite growth is in priority from the viewpoint of attractive force. Perhaps it is this reason that led to the crystallite size became large again that was close to the LBT–PVP prepared without PVP.

Fig. 2.3-10 (b) shows the effect of PVP concentration on the PS of LBT–PVP prepared in different PVP concentration measured by FE-SEM and DLS respectively. Only LBT–

PVP prepared in 100 g/L PVP aqueous shows mono-dispersion, for the PS measured by FE-SEM (130 nm) and DLS (175 nm) was very close. And the size distribution measured by DLS is the narrowest than the other samples. These results indicate that there is optimum value PVP concentration to prepare mono-dispersion LBT–PVP. The PS of LBT–PVP measured by FE-SEM decreased with PVP concentration increasing, on the other hands the PS measured by DLS shows V-shape trend that the PVP concentration of 100 g/L being as the bottom point. These results demonstrate that the particles show different degree of aggregation except the BT–PVP prepared in 100 g/L PVP solution.

2.3.5 Effect of PVP molecular weight ($M_{w,}$ PVP)

In order to examine the effect of different molecular weight of PVP on LBT−PVP synthesis, particle growth, and particle dispersion, the PVP concentration was fixed at 50 g/L which the highest $M_{w,}$ *PVP* of 360,000 g/mol could be also dissolved at ambient temperature.

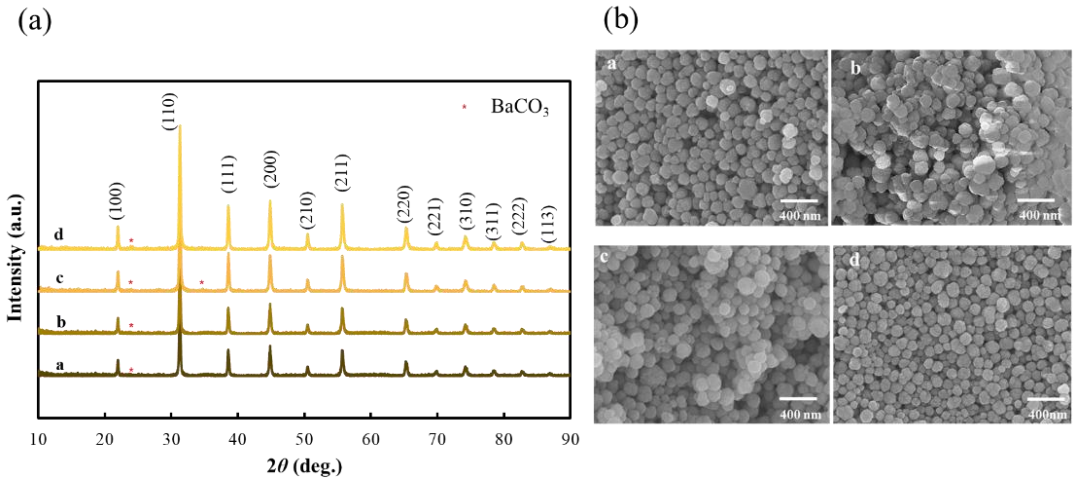

Fig.2.3-11 XRD diffraction pattern (a) and FE-SEM images (b) of LBT–PVPs prepared in different PVP molecular weight. (a) 2500, (b) 10000, (c) 40000, and (d) 360000 g/mol.

Fig.2.3-11(a) shows the XRD diffraction pattern of LBT–PVPs prepared with different PVP molecular weight. The phase of LBT-PVPs is cubic for a good agreement to JCPDS card No. 79-2263. The lattice parameter (4.04 Å) and crystallite size (~42 nm) were calculated as described in section 2.3.4, indicating that $M_{w,\ PVP}$ does not affect the crystallite size and lattice parameter in this PVP concentration. Fig.2.3-11(b) is their FE-SEM images. The spherical particles size around 140 nm, did not change with $M_{w,\ PVP}$ increasing. Table 2.3-2 was summarized these results in detail.

Table. 2.3-2. Results of LBT–PVP prepared with different molecular weights PVP. The concentration of PVP was 50 g/L.

Sample	$M_{w,PVP}$ (g/mol)	Lattice parameter (Å)	Crystallite size[a] (nm)	PS[b] (nm)	Crystalline No. in a particle
Mw1	2500	4.0469	45.5	143.8	32
Mw2	10,000	4.0428	44.5	141.0	32
Mw3	40,000	4.0433	43.1	143.5	36
Mw4	130,000	4.0444	42.2	151.5	46
Mw5	360,000	4.0432	42.3	132.2	31

[a] Calculated using Scherrer's equation.

[b] Measured by FE-SEM.

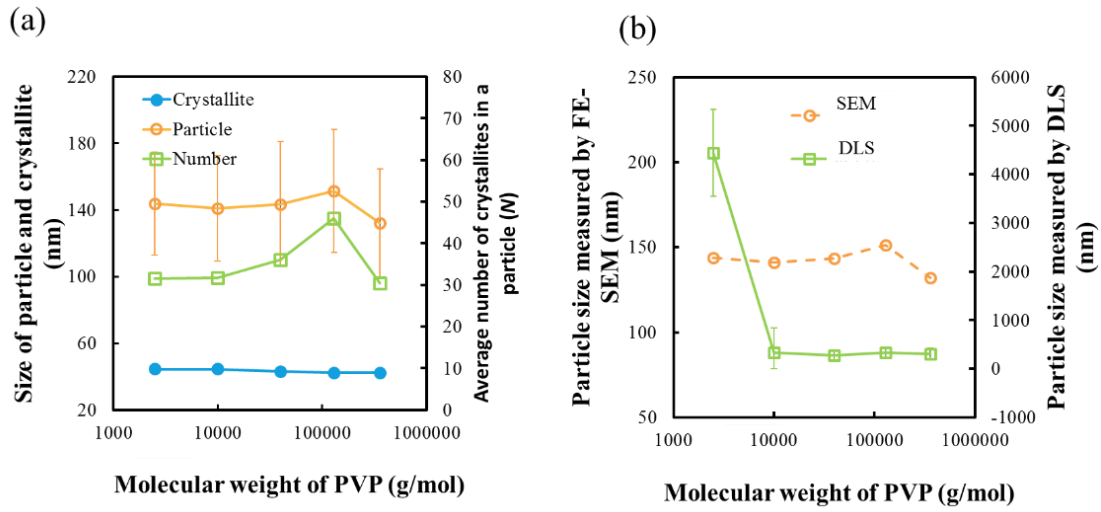

Fig. 2.3-12 (a) Effect of PVP molecular weigh on PS, crystallite size, and average number of crystallite in a particle of LBT–PVP. (b) Effect of PVP molecular weigh on the PS of LBT–PVPs measured by FE-SEM and DLS

As the section 2.3.4 described method, the number of crystallites in a particle was calculated, based on Table.2.3-2, Fig. 2.3-12 (a) were plotted. It can be observed that the PS (140nm), crystallite size (43 nm) and the number of crystallites (40 *N*) in a particle did not changed with the *Mw PVP* increasing. This result is different to Izu et al., [30] reported that the PS decreased with *Mw PVP* increasing, for the viscosity of reaction solution increase with molecular weight of polymer, and the particle growth was inhabited.The PVP concentration was too low in our study (50 g/L) that was less than half (120 g/L) of Izu et al., the viscosity of reaction solution was so low that the PVP network was not enough to affect the growth of particle and crystallite. These results indicate that the influence of *Mw PVP* appears after exceeding a certain PVP concentration.

Fig. 2.3-12 (b) shows the effect of *Mw PVP* on the re-dispersion of LBT–PVPs prepared in different *Mw PVP* reaction solution. The PS around 300 nm measured by DLS do not change with *Mw PVP* except the LBT–PVP prepared with 2500 g/mol, which is double of the results around 140 nm measured by SEM . These results indicate that the re-dispersion of the LBT–PVPs in aqueous solution were very high, and was not affected by *Mw PVP* as it above 10000 g/L in our study. But the LBT–PVP prepared 2500 g/mol demonstrated strong aggregation for the PS around 2500 nm which is very larger than that one around 140 nm measured by SEM. It indicates that the minimum *Mw PVP* is

essential to prevent aggregation of 140 nm LBT-PVP particles in aqueous solution.

2.4 Discussion

2.4.1. Mechanism of LBT–PVP nanoparticle growth

So far dissolution-precipitation [31] and in situ transformation [32] are proposed for the formation of BT nanoparticles. Base on the above experiment results it is believed that the formation of LBT-PVP nanoparticle follows the dissolution-precipitation mechanism in this study.

In our study we investigated the factors that influence the growth of particles from two aspects. One is the amount of nuclei of BT forming and the other is the environment of the nuclei existing. The amount of BT nucleus is relatively less as the concentration of Ti, Ba, and KOH was low in reaction solution. So the size of particle and crystalline are relatively large. But the amount of nucleus of BT increases with the concentration of Ti, Ba, and KOH increasing, results large number crystalline BT aggregated from nucleus exist in reaction solution. The particle growth would be inhabited by the large amount of small crystallite and results large number small nanoparticle in reaction solution as the classical nucleation and growth model. In the other hand, the growth of particle and crystalline have to migrate PVP to remove the hindrance from the network of PVP

molecules in reaction solution, and secure the growth space. The growth space become narrow with PVP concentration increasing for the network of PVPs becoming dense. It is common that the network of PVP increase with the $M_{w,}$ *PVP* increasing. However our results are not consistent with this inclination for the PVP concentration is too low to form PVP network in reaction solution. So It was found that $M_{w,}$ *PVP* did not affect the growth of crystalline and particle.

2.4.2. Mechanism of LBT–PVP nanoparticle dispersion

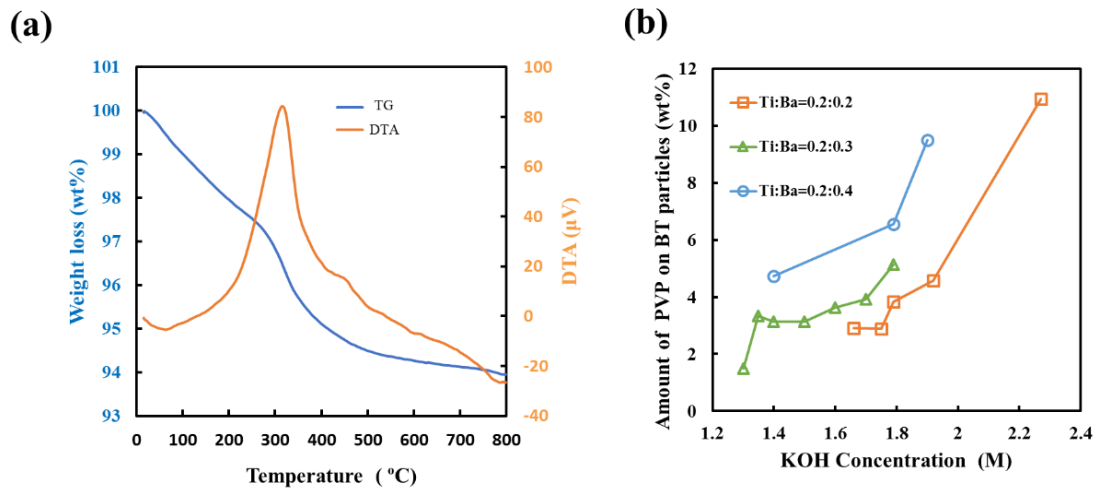

Fig. 2.4-1 (a) TGDTA pattern of LBT–PVP prepared in Ti: Ba = 0.2: 0.2, PVP= 100 g/L, KOH= 1.8 M, 80 ºC, 1h. (b) Relationship between the amount of PVP adsorbed on the surface and the KOH concentration.

Fig. 2.4-1 (a) is TGDTA curve of LBT–PVP prepared in standard condition. It demonstrates that there is amount of PVP on the surface BT, for there is weight loss (4.1

wt.%) around 200–800 ºC , and exothermic peak around 200– 400 ºC which is considered of PVP combustion [33]. The amount of PVP adsorbed on the surface BT prepared in different concentration of KOH reaction solution is plotted in Fig. 2. 4-1 (b). It can be seen that the amount of PVP increases with KOH concentration increasing, indicating that the KOH concentration not only affects particle growth, but also affects the amount of PVP adsorbed on the BT surface. In the other words that KOH indirectly affects the dispersion of LBT–PVP. From the Fig. 2.4-1(b) it can be seen that the amount of PVP is also increase with Ba concentration increasing at the same KOH concentration. It is thought that the PS decreased with Ba concentration increasing as the section.2.3.2 described, and led to an increase in total area of the particle surface. As a results, the amount of PVP adsorbed on LBT–PVP prepared in excess of Ba sources (0.3 and 0.4 M) were higher than that one prepared in Ti: Ba = 0.2: 0.2.reaction solution. It concludes that Ba is also affect the amount of PVP adsorption on the surface BT, and indirectly affect the dispersion of LBT-PVP.

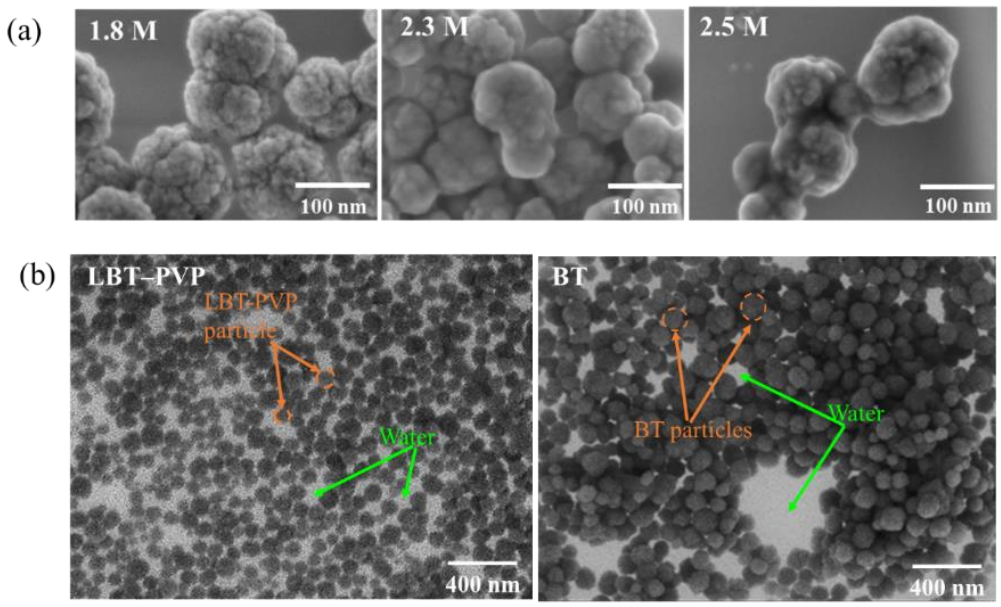

Fig. 2. 4-2 (a) FE-SEM Images of LBT-PVPs prepared in different KOH concentration reaction solution. (b) FE-SEM Images of LBT-PVP prepared with PVP and BT prepared without PVP in their 1 wt% suspension.

The morphology of PVP adsorbed on the BT was observed by FE-SEM with a low accelerating voltage of 2kV. In this observation condition, the PVP adsorbed on the surface BT was not transmitted. Fig. 2. 4-2 (a) shows the morphologies of PVP absorbed on the BT-PVP prepared in different KOH concentration reaction solution. The surface of LBT–PVP prepared in 1.8 M KOH solution was very rough, PVP could not be confirmed. It maybe that the amount of PVP on the surface BT was small around 4.1 wt %. As the KOH concentration increased the surface became smooth (2.3 M), and gel (2.5 M) for the amount of PVP increasing from 10 to 17 wt %. It was considered that the gel is a cross-

linked PVP through popcorn polymerization [34].

As described in previous section the BT prepared without PVP demonstrates strong aggregation among particles, on the other hand the LBT–PVP prepared in 100 g/L PVP solution showed mono-dispersion, for the PS is very close that measure by FE-SEM (130 nm) and DLS (175 nm) respectively. In order to directly observe the dispersion state of LBT-PVP in aqueous solution, the BT and LBT-PVP 1wt.% suspension were put into a new sample holder namely trans-SEM as Izu et al., [23] reported. Fig. 2. 4- 2 (a) shows the SEM images of their re-dispersion morphology. The particle is marked with orange circle line, and the water is marked with green arrow. It can be observed that the spherical dark dots of LBT–PVP nanoparticles are separated from each other and have no overlap, indicating that the LBT–PVP nanoparticles spread and single layer in the holder. On the contrary, the large dark particles aggregation, and overlapped to each other are observed for BT without PVP. These images indicated that the dispersion was realized by the PVP that adsorbed on the surface BT, and the aggregation cause from the attractive force among the particles.

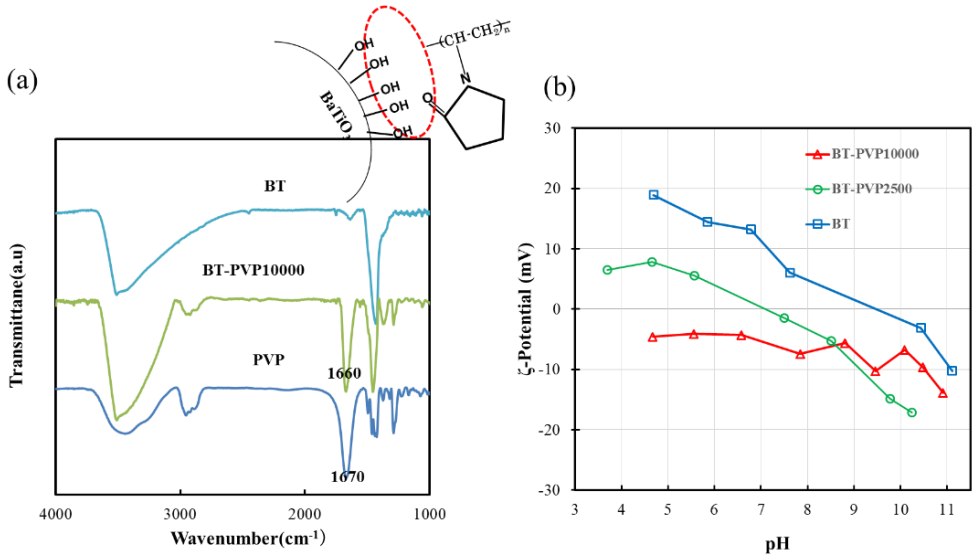

Fig. 2. 4-3 (a) FT-IR spectrum of BT, LBT–PVP 10000, and PVP. (b) Effect of pH on the zeta potential of the BT (prepared without PVP), BT–PVP10000 (prepared with 10000 g/mol PVP), and BT–PVP 2500 (prepared with 2500 g/mol PVP).

The chemical structure of PVP adsorbed on the BT surface, and interaction between PVP and BT were investigated by FT-IR. Fig. 2. 4-3 (a) is the FI-IR spectrum of BT, BT-PVP10000, and PVP. The chemical structure of PVP adsorbed on the BT was not decomposed in reaction, comparing with PVP and BT spectrums, indicating that PVP contributed to the dispersion of BT while maintained its own chemical structure. But the stretching vibration peak of C=O [35] slightly shifted to the lower wavenumber 1660cm^{-1} than PVP's(1670cm^{-1}). It also can be observed the stretching vibration peak of OH around 3400cm^{-1} for the BT without coated by PVP. As the monodispersed PVP-coated ZnO in an alkali solution reported [36], BT–PVP was also guessed that the surface of BT

was attached by a large quantity hydroxide ion (OH^-) in an alkali solution, and lead to the peak (C=O) slightly shift to low wavenumber as the inset illustration of their interaction.

It is well known that PVP as a dispersant can be prevent nanoparticles aggregation. [28] As the section 2.3.4 and 2.3.5 described, the particles of BT (prepared without PVP) , and LBT-PVP 2500 (prepared with 2500 g/mol) were strong aggregation for each other in their aqueous suspension, but the particles of LBT-PVP 10000(prepared with 10000 g/mol) demonstrates mono-dispersion in its aqueous suspension. In order to understand the dispersion mechanism of PVP, the electrostatic stabilization of BT, LBT–PVP2500, and LBT–PVP10000 were evaluated by the zeta potential via the charge at the particle surface of an electrical double layer in their aqueous suspension. The isoelectric point (IEP) is the pH where the charge of anions and cations are equal in solution. The IEP is a useful value to understand the particles behaviour in suspension. The true IEP of BT is around pH= 6.5 has been reported by M.C. Blanco-Lopez et al., [37] the IEP of ceramic oxide fluctuates within the range of ± 2 strongly depends on the source material and synthesis condition [38,39]. Fig. 2. 4-3 (b) shows the pH effect of suspension solution on their zeta potentials. The zeta potential of BT is from 20 to-20 mV with pH increasing, and the IEP is at pH=9. The PS of BT was about 200 nm, and prepared in the aqueous solution, maybe this lead to the IEP slightly large. But the zeta potential of BT–PVP2500

prepared with 2500 g/mol PVP is from 10 to -20 mV with pH increasing, and the IEP is slightly shifted to low pH=7 value. This may be due to the surface of BT covered by PVP. But the amount and length of PVP was not enough to prevent the aggregation of nanoparticles, so the zeta potential of BT–PVP2500 showed the similar behavior as aggregation of BT in aqueous. On the other hands the zeta potential of BT-PVP10000 is constant value around -4 and -10 mV without IEP, although pH changes from 4-10.It indicates that LBT–PVP10000 demonstrates extremely stability in aqueous suspension. The mono-dispersion of LBT-PVP10000 is realized by its steric effect for the PVP is nonionic dispersant. But minimum length of PVP is required to maintain mono-dispersion of LBT-PVP nanoparticle. So the length of molecular weight 2500 g/L PVP is too short to prevent the nanoparticles aggregation.

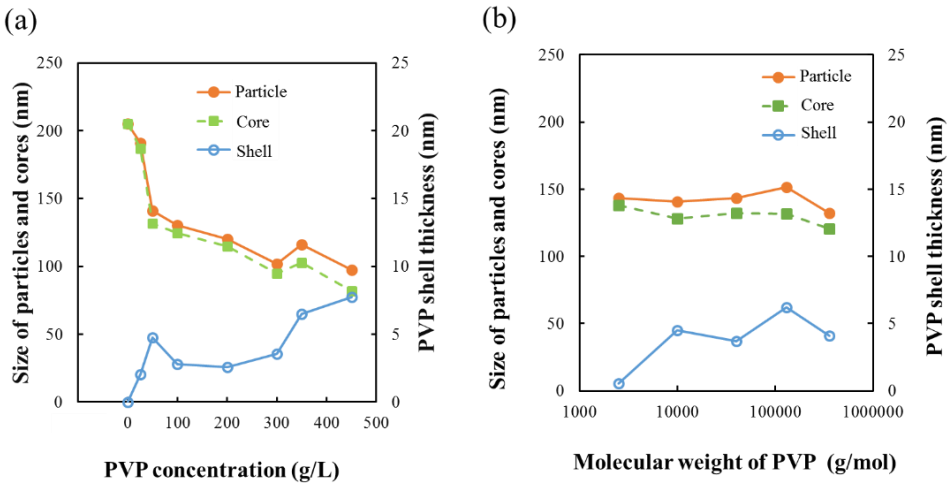

Fig. 2. 4-4. Effect of PVP concentration (a) and molecular weight (b) on the PS, core size and PVP shell thickness.

As Fig. 2. 4-2 (a) showing, the morphology of the surface of BT became smoother with amount of PVP increasing. So the nanoparticles of LBT–PVP was regarded to be core (BT) –shell (PVP) structure. In order to quantitatively understand the dispersibility of PVP, the shell thickness of PVP was evaluated by the under equations (1) and (2) as the Izu et al., [30] reported

$$W_L = \frac{\left[\frac{4}{3}\pi\left(\frac{d_c}{2}+t_s\right)^3 - \frac{4}{3}\pi\left(\frac{d_c}{2}\right)^3\right]D_s}{\left[\frac{4}{3}\pi\left(\frac{d_c}{2}+t_s\right)^3 - \frac{4}{3}\pi\left(\frac{d_c}{2}\right)^3\right]D_s + \left[\frac{4}{3}\pi\left(\frac{d_c}{2}\right)^3\right]D_c} \times 100\% \quad , \quad (1)$$

$$d_{cs} = d_c + 2t_s \qquad (2)$$

W_L is the amount of PVP that absorbed on the surface BT which evaluated by weight loss of TG data from 200 to 700 ºC. d_s and t_s represent the diameter of BT core and the thickness of the PVP respectively. D_c and D_s represent the density of BT (6.02 g/cm^3) and PVP (1.66 g/cm^3 [40]). d_{cs} is the diameter particle LBT–PVP.

Fig. 2. 4-4(a) shows the effect of PVP concentration on the PS, core size and the shell thickness. The size of particle and core decreased with the PVP concentration increasing. And the shell thickness increased from 2.0 to 7.7 nm as the PVP concentration increased from 25 to 450 g/L. It was known that the LBT–PVP prepared at 100 g/L PVP solution

demonstrated mono-dispersion, as Fig. 2.3-6 (b) showing. The shell thickness was just 2.8 nm, indicating that the PVP shell was very thin. Maybe, the PVP molecules easily spread for the thin PVP shell in solution, and maintain the high dispersion of LBT–PVP via the PVP steric effect. If the thickness of PVP shell is thinner than 2.8 nm the agglomeration was caused by the attractive force of the nanoparticle surface of LBT–PVP. And as the thickness of PVP shell is thicker than the 5 nm the agglomeration was caused by cross-linking of PVP.

Fig. 2. 4-4(b) shows the effect of PVP molecular. The size of particle and core did not change with M*w PVP* increasing. And the thickness of PVP shell did not change around 5 nm except the LBT–PVP prepared with 2500 g/mol PVP. It indicates that the high dispersion is maintained by the thin layer although M*w PVP* increasing. The length of PVP was very longer than the shell thickness. It maybe that the PVP was adsorbed on the BT surface with many loops.

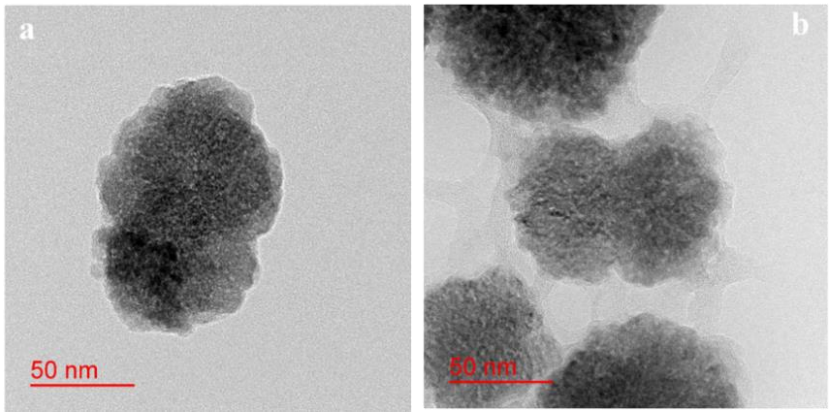

Fig. 2.4-5 TEM images of BT-PVP prepared in different PVP concentration.(a): PVP=

100g/L, (b): PVP=400 g/L

The thickness of PVP is around 2-8 nm with different concentration and molecular weight of PVP. Especially the thickness of mono-dispersion BT-PVP prepared with 100g/L is around 2.8 nm, but the layer of PVP could not be observed in its TEM image showing in Fig. 2.4-5(a). It indicates that the most of PVP is involved into the particle, and only a small part of PVP remains on the particle surface with particles growth. The small part of PVP is the optimum amount to prevent the aggregation of BT nanoparticle. As PVP concentration increases, it is observed that PVPs were entangled as Fig. 2. 4-5(b) showing, indicating that the aggregation cause from the PVP entanglement.

2.5 Conclusion

High dispersion spherical BT–PVP nanoparticles were prepared at ~80 °C using $TiCl_4$, $BaCl_2$, and PVP in an aqueous reaction solution with a single-step. The effect factors on the growth and the dispersion of the cubic nanoparticle LBT–PVP were investigated, such as temperature, time, raw material concentrations, KOH concentrations, PVP concentrations, and molecular weight of PVP. These factors mainly from two aspects directly or indirectly affect the growth of particles: one is the amount of BT nucleus

formation such as concentration of Ba, Ti, and the other is BT nucleus existing environment such as concentration of KOH, PVP and M*w PVP*. It is found that mono-dispersion of BT–PVP that the PS was 114 nm analyzed by FE-SEM could be prepared the optimum condition by using a [Ti]/[Ba] molar ratio of 0.2:0.3 , [KOH] of 1.4M, and 10000 g/mol [PVP] of 100 g/L. There is optimum condition synthesis for high dispersion LBT-PVP shows in Fig. 2.5-1 with pale green. The aggregation of nanoparticle BT-PVP is via attractive force in the agglomeration area with white color, and the aggregation is via PVP entanglement in the gel area with dark green.

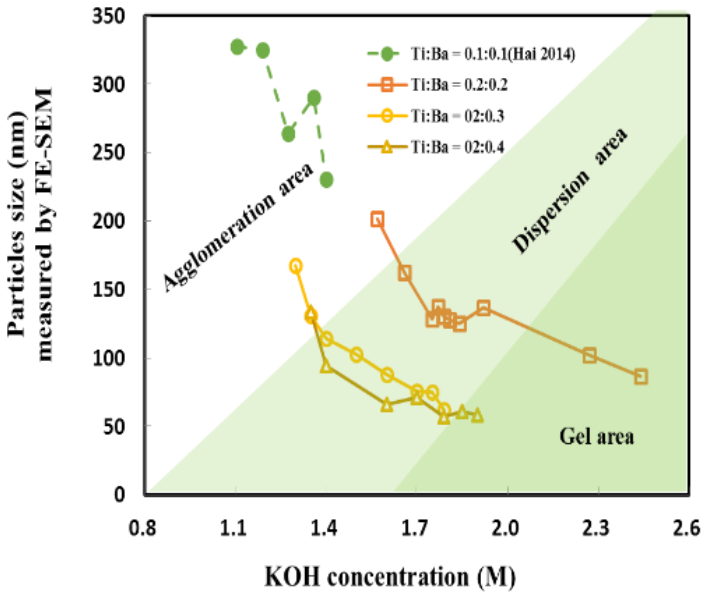

Fig. 2.5-1 Relationship between PS and KOH concentration at different of concentration ratios.

At the same time the dispersion mechanism was investigated. High dispersion of LBT–

PVP realizes by physical adsorption and the steric effect of dispersant PVP. And the dispersion state in solution was directly observed by the FE-SEM with a new holder. Through comparing the shell thickness of core-shell LBT-PVP nanoparticle to theirs TEM image, it confirmed that most part amount of PVP exists inside of particle. KOH concentration indirectly affects the amount of PVP adsorbed on the BT surface. And the effect of M*w PVP* on the particle growth and dispersion of LBT– PVP have to exceed the critical concentration that the PVP molecules form network in reaction solution.

2.6 References

[1] G. Arlt, D. Hennings, G. de with, *J. Appl. Phys*., 58,1619–1625 (1985).

[2] A.D. Hilton, R. Frost, Recent development in the manufacture of $BaTiO_3$ powders, in: Key Engineering Materials, Vols. 66–67. Trans Tech Publications, Zurich, Switzerland, 1992, pp. 145–83.

[3] L.E. Cross, Dielectric, piezoelectric and ferroelectric components, *Am. Ceram. Soc. Bull.* 1984, 63, 586–90.

[4] D. Pandey, A.P. Singh, V.S. Tiwari, Developments in ferroelectric ceramics for capacitor applications, *Bull. Mater. Sci.* 1992, 15, 391–402.

[5] G. Arlt, D. Hennings, G. de With, *J. Appl. Phys*. 1985, 58, 1619–1625.

[6] X. Deng, X. Wang, H. Wen, L. Chen, L. Li, *Appl. Phys. Lett.* 2006, 88, 252905.

[7] Y. He, *Thermochim. Acta*. 2004, 419, 135–141.

[8] M.H. Frey, D.A. Payne, *Chem. Mater.* 1995, 7, 123–129.

[9] A.V. Prasadarao, M. Suresh, S. Komarneni, *Mater. Lett*. 1999, 39, 359–363.

[10] S. Wada, T. Tsurumi, H. Chikamori, T. Noma, T. Suzuki, *J. Cryst. Growth.* 2001, 229, 433–439.

[11] S. Venigalla, D.J. Clancy, D.V. Miller, J.A. Kerchner, S.A. Costantino, *Am. Ceram. Soc. Bull*, 1999, 10, 51–54.

[12] J.H. Jean, H.R. Wang, *J. Mater. Res.* 1998, 13, 2245–50.

[13] J.H. Jean, H.R. Wang, *J. Am. Ceram. Soc.*1998, 81, 1589–99.

[14] A.R. Tao, S. Habas, P. Yang, *Small*. 2008, 4, 310–325.

[15] N. Izu, T. Uchida, I. Matsubara, T. Itoh, W. Shin, M. Nishibori,, *Mater. Res. Bull*. 2011, 46, 1168–1176.

[16] M.A. Lopez-Quintela, Curr. *Opin in Colloid & Interface Sci*., 2003, 8, 137–44.

[17] S. O'Brien, L. Brus, C.B. Murray, *J. Am. Chem. Soc*. 2001, 123, 12085–86.

[19] T.J. Trentler, T.E. Denler, J.F. Bertone, A. Agrawal, V.K. Colvin, *J. Am. Chem. Soc.* 1999, 121 1613–14.

[20] J. Park, K. An, Y. Hwang, J.-G. Park, H.-J. Noh, J.-Y. Kim, J.-H. Park, N.-M. Hwang,

T. Hyeon, *Nature Mater*. 2004,3, 891–95.

[21] M. Iijima, N. Sato, M. Tsukada, H. Kamiya, *J. Am. Ceram. Soc.* 2007, 90, 2741–2746.

[22] C. Hai, K. Inukai, Y. Takahashi, N. Izu, T. Akamasu, T. Itoh, W. Shin, *Mater. Res. Bull.* 2014,57, 103–109.

[23] N. Izu, T. Ogura, T. Akamatsu, T. Itoh, W. Shin, *Ceram. Inter.* 2014, 40, 16361–16364.

[24] S. Wada, Chikamori. H, Noma. T, Suzuki, *J. Mater. Sci. Lett.* 2000, 19, 283–285.

[25] X. Li, W.H. Shin, *J. Am. Ceram. Soc*. 1997, 80, 2844–2852.

[26] H. S. Lee, S.M. Koo, J.W. Yoo, *J. Mater. Sci. Eng., A*, 2012, 2, 7–15.

[27] B.L. Newalkar, S. Komarneni, H. Katsuki, *Mater. Res. Bull*. 2001, 36, 2347–2355.

[28] Y. Sun, B. Mayer, T. Herricks, Y. Xia, *Nano Lett*. 2003, 3, 955–960.

[29] T. Ashida, K. Miura, T. Nomoto, S. Yagi, H. Sumida, G, Kutluk, K. Soda, H. Namatame, M. Taniguchi, *Surf. Sci.* 2007, 601, 3898–3901.

[30] N. Izu, T. Uchida, I. Matsubara, T. Itoh, W. Shin, M. Nishibori, *Mater. Res. Bull.* 2011, 46, 1168–1176.

[31] J.O. Eckert Jr., C.C. Hung-Houston, B.L. Gersten, Malgorzata M. Lencka, R.E Riman, *J. Am. Ceram. Soc.* 1996, 79, 2929–59.

[32] F. Dang, K. Mimura, K. Kato, H. Imai, S. Wada, H. Haneda, M. Kuwabara, *Nanoscale*, 2012, 4, 1344–1349.

[33] Y. Hao, X. Wang, H. Zhang, Z. Shen, L. Li, *J. Ceram. Soc. Jpn*, 2013,121, 506–511.

[34] F. HAAF, A. SANNER, and F. STRAUB, Poly J., 17, 143–152 (1985).

[35] S. Horiuchi, T. Hanada, N. Izu, I. Matsubara, *J. Nanopart. Res. 2012,* 14, 734(1)–(10).

[36] Waqar Ahmed, Nasar Ali, "Manufacturing nanostructurecha" Chapter 4 "Polymer-surfactant interactions and their influence on zinc oxide nanoparticles morphology" Marta Fiedot, Olga Rac, Patrycja Suchorska-Wozniak, Iwona Karbownik, Helena Teterycz, P124

[37] M.C. Blanco-Lopez, B. Rand, and F.L. Riley, *J. Eur. Ceram. Soc.* 2000, 20, 107-118.

[38] G. Parks, *Chem. Rev*. 1965, 65,177–198.

[39] J.S. Reed, Principles of Ceramic Processing, 2nd. John Wiley and Sons, New York, 1995, p. 152

[40] B.D. Vogt, Cl. Soles, H.J. Lee, E.K. Lin, W. Wu, *Polymer.* 2005, 46, 1635–1642.

3. High dispersion tetragonal $BaTiO_3$ synthesis and evaluation

3.1 Introduction

It is well known that $BaTiO_3$ (BT) is widely applied to multilayer ceramic capacitors (MLCCs), piezoelectric transducers, because for its ferroelectricity [1-3] and piezoelectricity [4-6]. The dielectric layers of MLCCs becomes thinner and thinner with the market requirement of miniaturization of electronic devices. It is very important to synthesize highly disperser nanoparticle of tetragonal BT to ensure the performance of miniature electronic components. But it is limited to synthesize highly disperse cubic BT nanoparticles under atmospheric pressure and low temperature condition as the chapter. 2 described.

The tetragonal BT nanoparticle is mainly prepared by solid-phase and liquid-phase methods in recently years. Comparing with solid-phase method, the hydrothermal as a one of liquid method can be easily prepared tetragonal nanoparticle BT with narrow size distributions [7-10] at much lower reaction temperatures. The drawback of OH lattice defect in aqueous reaction solutions could be suppressed by replacing organic solvent [11] or adding several percent organic solvent in aqueous reaction solutions [12, 13]. It is also indispensable of dispersant to maintain highly disperse nanoparticle BT.

Polyvinylpyrrolidone was also used here as low temperature process under atmospheric pressure. It is concerned whether the PVP decomposes in the high temperature and pressure of hydrothermal method, and how changes of crystal phase with reaction temperature and time.

In this section in order to prepare highly disperse tetragonal BT in a single step, a new PVP –assisted hydrothermal was developed that PVP was added with raw material into reactor. It is referred to HBT-PVP. The crystal phase and particle morphology with reaction temperature and time was investigate by X-ray diffraction, Transmission electron microscopy (TEM), high-resolution TEM (HRTEM) image. The chemical structure of PVP was analyzed by Fourier transform infrared spectroscopy (FT-IR). In addition, the mechanism of the observed particle dispersion and growth was discussed.

It is well known that the mechanism of BT growth in hydrothermal is mainly two proposed: one is in-situ reaction and the other is dissolution-precipitation [14, 15]. In order to understand the role of these two theories in this study, two different Ti starting materials mixed by $TiCl_4$ and TiO_2 were used. And the ratio of TiO_2 in Ti staring material were evaluated by the particle size and tetragonality of HBT-PVP. Furthermore the effects of reaction time and PVP concentration on the particle size, tetragonality, and dispersibility of HBT-PVP synthesis with TiO_2 as staring material were also investigated.

3.2 Experiment

3.2.1 Materials

The reagents ($TiCl_4$, $BaCl_2 \cdot 2H_2O$, KOH, PVP) are same as section 2.2.1 described. The details of reagent grade and supplier refer to this section.

3.2.2 Synthesis

The materials of 0.2 M $TiCl_4$, 0.32 M $BaCl_2 \cdot 2H_2O$, 100g/L PVP and 2.3 M KOH were put into a 50 mL Teflon container under constant stirring. The mixture solution was consisted with EtOH and distilled water in the volume ratio of 1:3. The total volume of reaction solution was 40 vol% of the 50-mL Teflon container. The Teflon container was sealed and set into autoclave. The synthesis was performed in desired temperature and time. The reaction factors was summarized in Table.3.2-1. After reaction, it was cooled to room temperature, and the precipitation was obtained by centrifugation via removing supernatant. The precipitation was washed with distilled water and EtOH, and dried at 60 ºC for 24h.

Table.3.2-1. Reaction factor of HBT-PVP synthesis with $TiCl_4$ as starting material

Factor	Temperature (ºC)	Time (h)	PVP concentration (g/L)
Temperature	150, 170, 190, 210, 230	24	100
Time	24	1, 5, 9, 21, 24	100

Furthermore, difference Ti sources used in synthesis were also summarized in Table.3.2-2.

Table.3.2-2. Reaction factor of HBT-PVP synthesis with $TiCl_4$ and TiO_2 as starting material

Reaction Parameter	TiO_2 (mol %)	Reaction Time (h)	PVP Concentration (g/L)
Content of TiO_2 in $TiCl_4$	0, 1, 2, 10, 50, 100	24	50
Time	100 (TiO_2)	5, 10, 24	50
	0 ($TiCl_4$)	5, 24	
PVP concentration	100	24	0, 1, 5, 50, 100, 200, 250

3.2.3 Characterization

The peak of (200) plane of HBT–PVP in XRD pattern was fitted with Guassian curve to split into (200) and (002). The lattice constant of **a** and **c** was calculated with Scherrer's Equation with the (200) and (002) plane. The tetragonality of BT–PVP was calculated by **c** divided by **a**. The other instrument of analysis and measurement was same as section 2.2.3 used. The details refer to the section 2.2.3.

3.3 Results and discussion

3.3.1. Effect of reaction temperature, time on particle growth of HBT-PVP

It has been reported that tetragonal BT can be prepared by hydrothermal in 240 ºC [16]. And the adding several percent of organic solvent into the reaction solution can be

improved the tetragonality of BT via suppressing the defect of BT which causing the OH group in hydrotherml process [12]. The mixture solution of EtOH and distilled water and dispersant PVP were used to prepared high dispersion tetragonal HBT–PVP. The mechanism of the particle growth was clarified from two reaction factors of temperature and time.

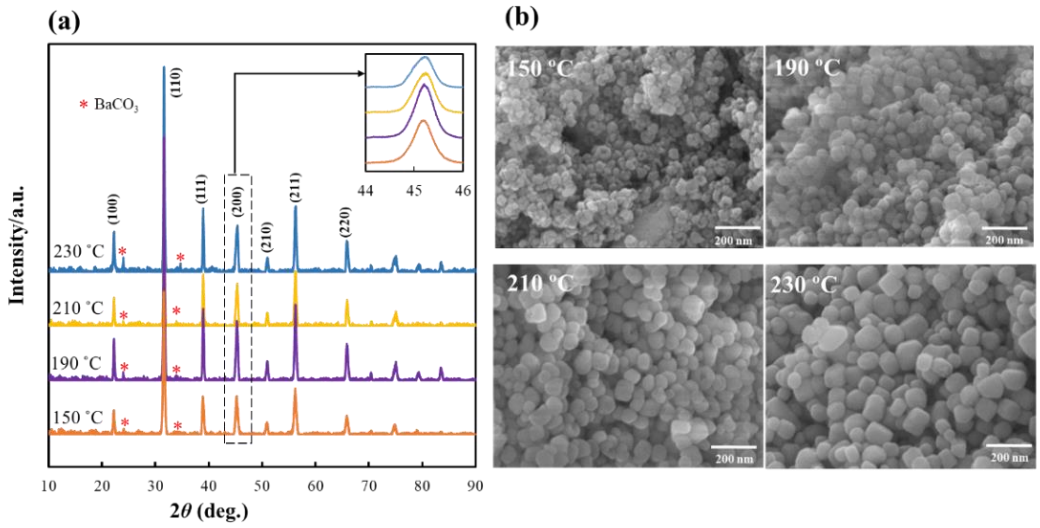

Fig. 3.3-1 XRD (a) and FE-SEM (b) images of BT–PVP prepared in different temperature for 24h. (a)150 ºC,(b)190 ºC, (c) 210ºC, (d)230 ºC. The inset is the XRD diffraction pattern from 44 to 46º.

Fig.3.3-1 (a) is XRD of HBT–PVPs prepared in different reaction temperature. The diffraction patterns of HBT–PVP prepared at 150 and 190 ºC are in good agreement to the PDF card No: 01-079-2263, indicating that its crystalline phase are cubic. And the

crystalline phase of those prepared at 210 and 230 ºC are tetragonality for its XRD patterns agree to the PDF card No. 01-079-2264. These results indicate that the phases of HBT–PVP depends on the reaction temperature in hydrothermal, and the high temperature is advantage to form tetragonal phase. It is also can be observed that weak intensity peak of $BaCO_3$ marked with red asterisk in XRD diffraction pattern. It is inevitable that the small amount of impurity $BaCO_3$ being in our samples for CO_2 present in atmospheric air and reaction solution. The tetragonal BT–PVP can be obtained above 210 ºC, although the splitting peak of (200) does not be observed in the inset of the XRD pattern around 44- 46º, but the peak was slightly wider than that prepared at 150, 190 ºC. It is speculate that the two split constitute the (200) plane peak. Fig.3.3-1 (b) is the FE-SEM images of these HBT-PVPs prepared from 150 to 230 ºC. The particle size of HBT-PVPs prepared at 150 and 190 ºC is very small around 50 nm, and showed torus-like shape. As the temperature increases to 210 ºC the particle size becomes large around 80 nm, the ring of the torus becomes thick and the hole of the center became small. At last the center of the torus-like particle is completely filled up and grows into large cube shape around 83 nm at the 230 ºC.

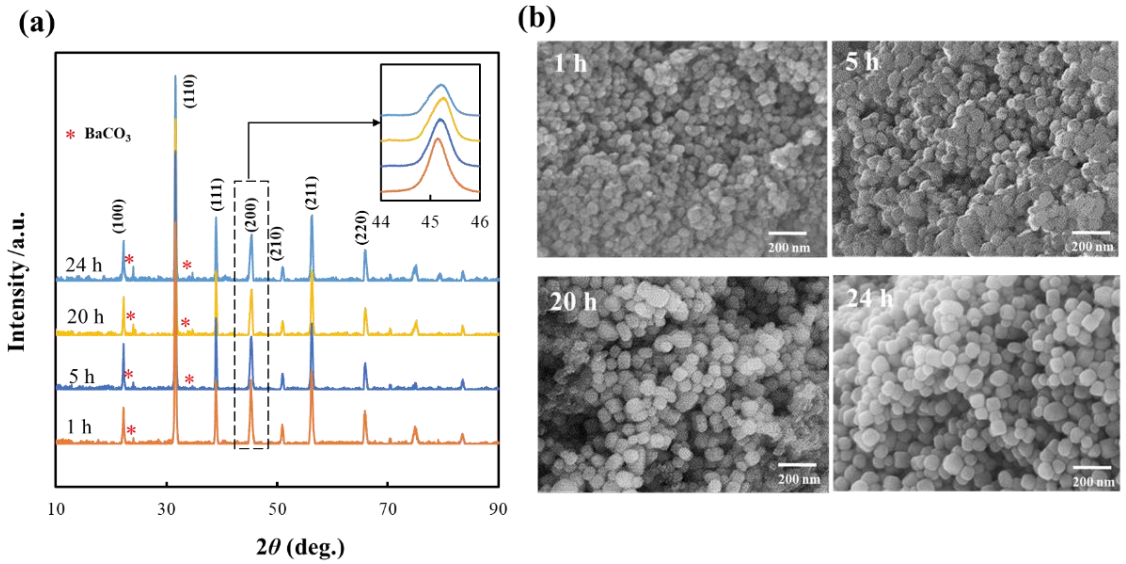

Fig. 3.3-2 XRD (a) and FE-SEM (b) images of HBT–PVP prepared for different reaction time in 230 ºC. The inset is the XRD diffraction pattern from 44 to 46º of 2θ.

Fig.3.3-2 (a) is the XRD pattern of the HBT–PVPs prepared for different reaction time. The phase of HBT–PVPs prepared for 1, 5h were cubic for its XRD pattern matches to PDF No. 01-079-2263. And the phase of BT–PVPs prepared for 20, 24 h are tetragonal for their XRD pattern matches to PDF card No 01-079-2264. As the section 3.3.3.1 described the split peak of (200) plane of the tetragonal HBT–PVPs are not observed but become wide with reaction time in the inset of XRD pattern around 44-46º. These results demonstrate that the reaction time also affect the phase of HBT–PVP. The tetragonal HBT–PVP could be prepared above 20 h. Fig.3.3-2 (b) is the FE-SEM images of these

HBT–PVPs particles. The HBT–PVP prepared for 1h was spherical small particle around 50nm. Several small ring-shaped particles were also observed in the image. The morphology of HBT–PVP particle changed from spherical to cube, and the particle size became large to 80 nm with reaction time. These results indicated that the particle growth is affected by the reaction time.

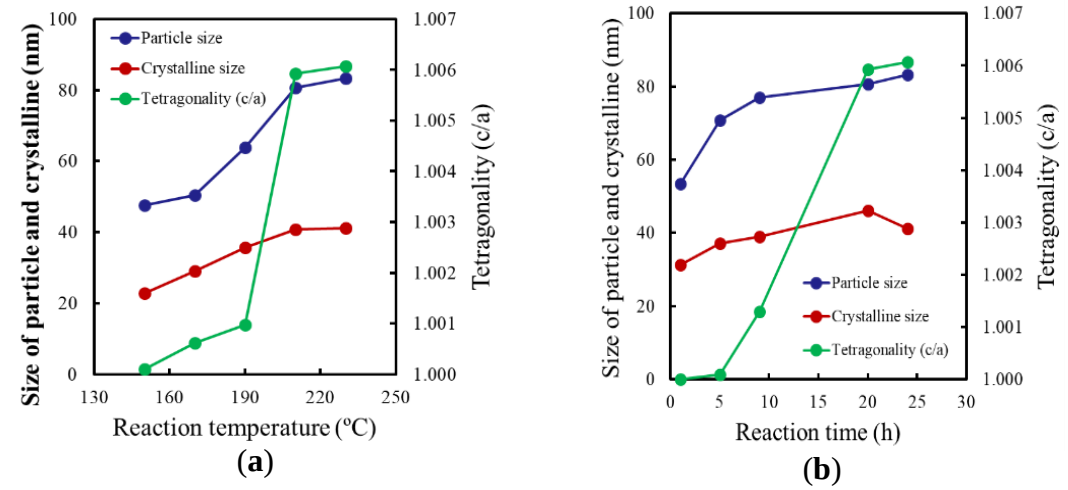

Fig. 3.3-3 Effects of temperature (a) and time (b) on particle size, crystalline size and tetragonality of HBT–PVP. The tetragonal is calculated as the 3.2.3 section described.

The effect of temperature is plotted in Fig.3.3-3 (a). The crystallite size increases from 20 to 40 nm that calculated by Scherrer's Equation with the full width at half maximum (FWHM) of the (110) diffraction peak in XRD pattern, and the particle size increases from 50 to 83 nm measured by SEM image with reaction temperature increasing. These

results reveal that a particle is consisted with several number of crystallites about 5-9. So the nanoparticle HBT–PVP prepared hydrothermal method have a high crystallinity comparing with prepared in low temperature under atmospheric pressure. It has been reported that the tetragonal BT can be observed split two peak of (002) and (200) planes around 44–46º [17, 18]. The peak of the (200) plane were fitted with the Gaussian function, and separate into two peaks of (200) and (002) plane as reported Kwon et al [12]. The lattice parameters ***a*** and ***c*** are calculated and the tetragonality of HBT–PVP particles is evaluated using the c/a value. The tetragonality of the HBT–PVPs increases from 1.0001 to 1.0061 and rapidly increase around 190 and 210 ºC as Fig. 3.3-3 (a) showing. It indicates that the tetragonality of HBT–PVP is affected by reaction temperature as reported by Uchino et al [19]. It also demonstrate that the crystallite critical size of HBT–PVP phase is around 35 nm. The size is slightly larger than that Hoshina et al., [20] reported about 30 nm of the BT phase remained cubic. It may be related to the PVP in reaction system.

The effect of the reaction time was plotted in Fig.3.3-3 (b). The particle size increases from 53 to 77nm as the reaction time was changed from 1 to 9 h. After that it is almost constant around 80 nm although the reaction time is further longer. At the same time the crystallite size also increase from 30 to 40 nm that calculated from the FWHM of the

corresponding peal of (110) plane in XRD diffraction pattern. This indicates that a particle is consisted by several crystallites. The tetragonality (c/a) increases from 1.001 to 1.0061 with reaction time increasing. Especially, the value of tetragonality increasing is remarkable around 9-20 h. The phase of HBT–PVP change from cubic to tetragonal in this range. The crystallite size of HBT-PVPs prepared in 9 and 20 h are 39 and 46 nm. This indicates that the critical size is around 40 nm.

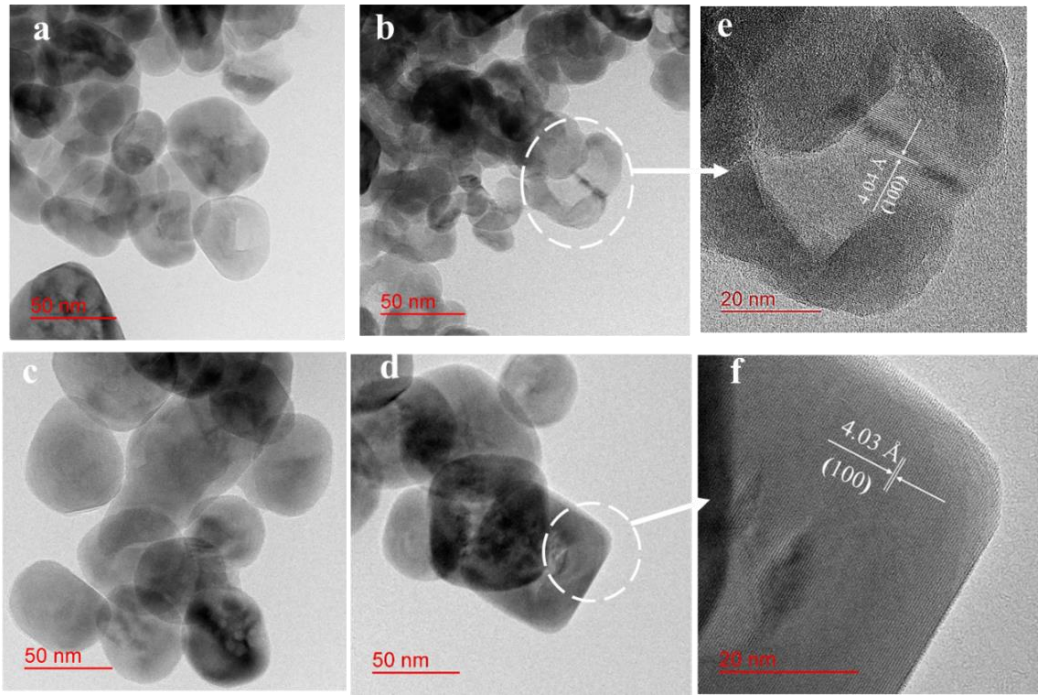

Fig. 3.3-4 TEM (a, b, c, d) and HRTEM (e, f) images of HBT–PVP prepared in different temperature and time. The condition prepared of HBT–PVP is (a) 230 ºC and 1 h, (b) 150 ºC and 24 h, (c) 230 ºC and 5 h, (d) 230 ºC and 24 h. **e** and **f** are the particle marked with white circle dashed line in **b** and **d** respectively.

Fig.3.3-4 shows the TEM (a, b, c, d) and images of the HBT–PVP particles synthesized at various reaction temperatures and times. The particle size increases with the reaction time as the order of the figure.3.3-4(a, c, d) showing. The particle average size is 35, 60, to 80 nm respectively. The particle morphology changes from semi-round, donut-like ones to round-cube and cube ones. These results indicate that the particle growth is affected by reaction time. The temperature effect was also observed. Figure.3.3-4(**b)** shows the particle prepared in 150 ºC. There are many donut-like ones in the images. As the reaction temperature increasing, the particle size increase and the hollow of the donut-like ones is filled up, grows into cube morphology as the figure.3.3-4(**d)** showing. The HRTEM image of figure. 3.3-4(**e)** shows the one of donuts-like particles marked with white dashed circle line in figure .3.3-4(**b)**. The homogenous lattice fringe of (110) plane is observed in the center area, indicating that the center of the donut-like particle is not empty, the center density of BT relatively lower than the outside one. And the Figure. 3.3-4(**f**) shows the particle marked with white dashed circle line in figure.3.3-4(d). The homogenous lattice fringe of (100) plane is observed in the whole of the particle indicating that the particle grows into single crystal. These results suggest that the donuts-like particle that prepared in low temperature and short time are filled up by the solid phase with reaction temperature and time. Although it has been reported that the torus

hole was filled up due to the diffusion of low-density crystallites from the torus center to the outside [21], but it is thought that the particle growth of HBT–PVP diffused from outside of high density crystallites to the inside of hole center in our study. And at last the HBT-PVP particle grows into single crystal with reaction temperature and time.

3.3.2 Effect of difference Ti source on particle growth of HBT-PVP

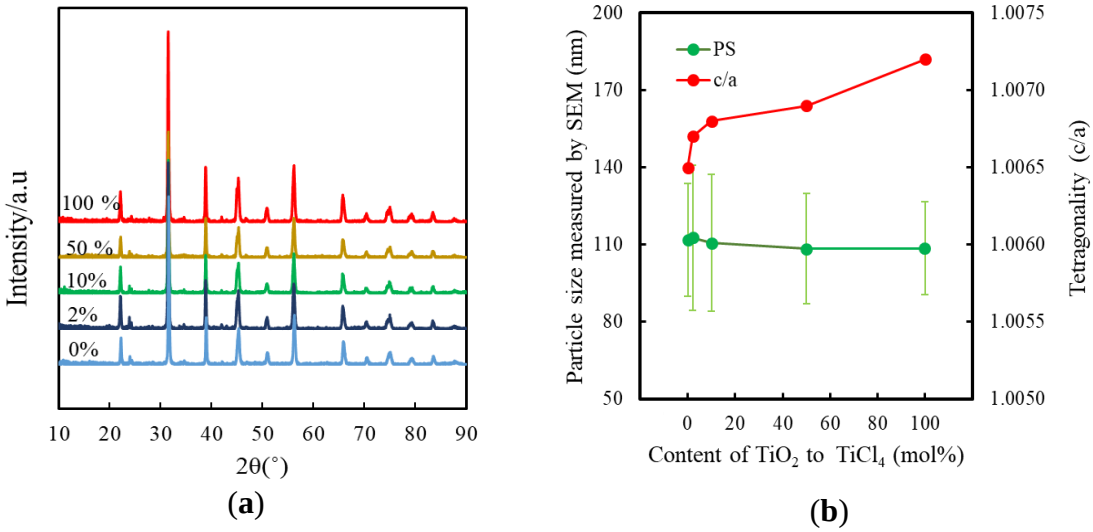

Fig. 3.3-5 (a) XRD diffraction pattern of BT-PVPs prepared in different ratio of TiO_2. (b) Effect of the TiO_2 ratio in the mixed source with TiO_2 and $TiCl_4$ on the particle size and tetragonality of HBT-PVP.

In order to evaluate the effect of TiO_2 sources, the reaction were prepared in aqueous solution. The total concentration of Ti mixed with TiO_2 and $TiCl_4$ is 0.2M. the other material concentration is 0.32M $BaCl_2 \cdot H_2O$, 100g/L PVP and 2.3M KOH. These

materials were mixed in aqueous and reacted in 230 ºC for 24h. Figure. 3.3-5 (a) shows XRD pattern of BT-PVPs prepared in different ratio TiO_2. The phase of these BT-PVPs is tetragonal and not change with the TiO_2 contents. The tetragonality is evaluated by the diffraction peak around 44 – 46 º. Figure. 3.3-5 (b) shows the effect of TiO_2 ratio in Ti sources on the particle size and tetragonality (c/a) of BT-PVP. It can be seen that the particle size is 110 nm, does not change so much, but the tetragonality (c/a) increases from 1.0057 to 1.0072 with the TiO_2 ratio increasing from 0 to 100 mol %. It indicates that the tetragonality increase although the particle size does not change in our study. In the other words that the higher tetragonality BT can be prepared by TiO_2 than $TiCl_4$ in PVP aqueous solution.

It is thought that the particle size is slightly decreases is due to the difference reaction mechanism. Wada et al., [22] and Joung et al., [23] proposed two-step growth mechanism of BT. The BT-PVP prepared with TiO_2 is similar to the proposal. Joung et al., obtained 95 nm BT at 260 ºC for 60h, its c/a is 1.0081. But the 108 nm HBT-PVP can be prepared at 230 ºC for 24h, furthermore there is no residual TiO_2 for the typical peak of 27.4º is not observed in their X-ray diffraction. It different from that Han et al., [24] reported. It is think that BT nucleation form in heterogeneously at the surface crystalline TiO_2, and relatively small particles of high tetragonality are grown with the help of TiO_2 substitution

in our study.

3.3.3. Effect of reaction temperature and time on dispersion of HBT–PVP particles

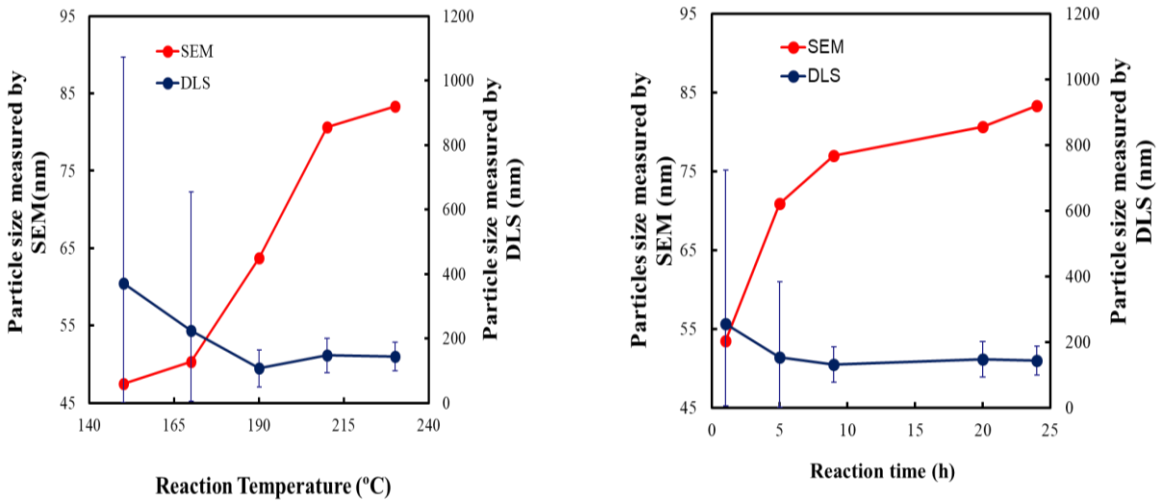

(**a**) (**b**)

Fig. 3.3-6 Effect of reaction temperature (a) and time (b) on the particle size measured by SEM and DLS respectively

In this section the dispersion of HBT–PVPs prepared in different time and temperature were investigated by comparing particle size measured by SEM and DLS respectively. The HBT-PVP is considered to have a mono-dispersion when the particle size are same in dry powder and in the solution. Fig.3.3-6 (a) shows the effect of reaction temperature on the particle size. The particle size measure by DLS decreases from 371 to 143 nm and the coefficient of variation (CV) decreases from 190 to 30 % with the reaction temperature increasing. As the reaction temperature is low, the particle size measured by

SEM is very small around 50 nm, but that measured by DLS is large around 350 nm and its size distribution is very wide, indicating that HBT–PVP have a strong aggregation. The particle size distribution become very narrow from 190 ºC, and the particle size of 106 nm is close to 63 nm of dry powder. This indicates that the HBT-PVP is mono-dispersion. Similarly the others prepared in 210 and 230 ºC also have a mono-dispersion. These demonstrate that the HBT–PVP have a mono-dispersion from 190 ºC. The effect of reaction time shows in Fig.3.3-6 (b). The particle size measured by DLS decreases from 255 to 143 nm with reaction time increasing. It demonstrates mono-dispersion from 9 h for the size distribution is very narrower (CV: 30 %) than that prepared in the short reaction time (CV: 180%).

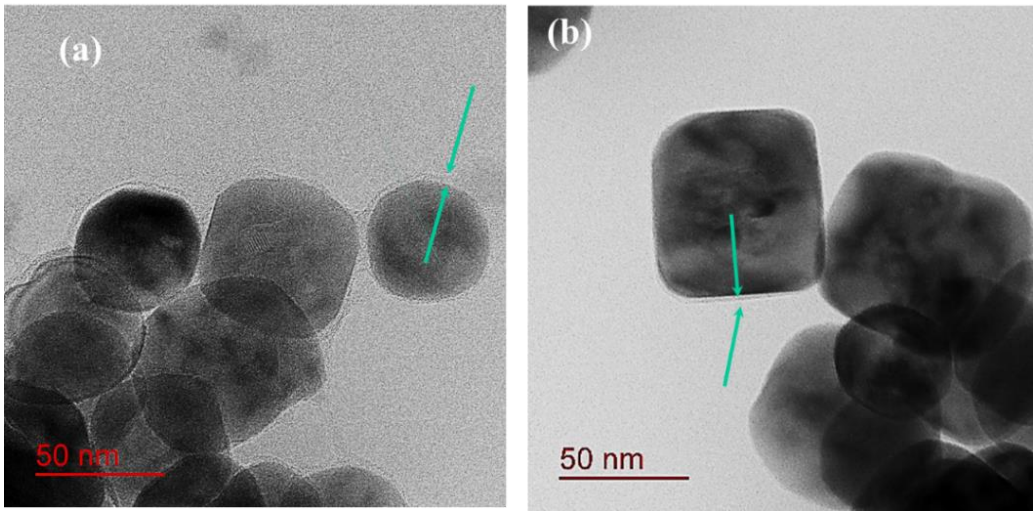

Fig. 3.3-7 TEM image of HBT–PVPs prepared in 230 ºC for 5h (a) and 24h (b).

Fig.3.3.-7 is the TEM images of HBT–PVPs prepared in different time. It can be

observed that the particle shows in two contrast. It indicates that the particle have a core-shell structure. The core is BT in dark contrast, and the shell is dispersant in light contrast for the lattice fringe is not observed, indicating that is amorphous organic matter. The shell thickness is 3.4 nm (Fig. (a)) and 2.6 nm (Fig. (b)) respectively that is consistent with their Tg results of 2.76 wt% and 0.91 wt%. It indicates that HBT-PVP prepared by hydrothermal is a core-shell structure. The organic matter contributes to the dispersion of HBT-PVP.

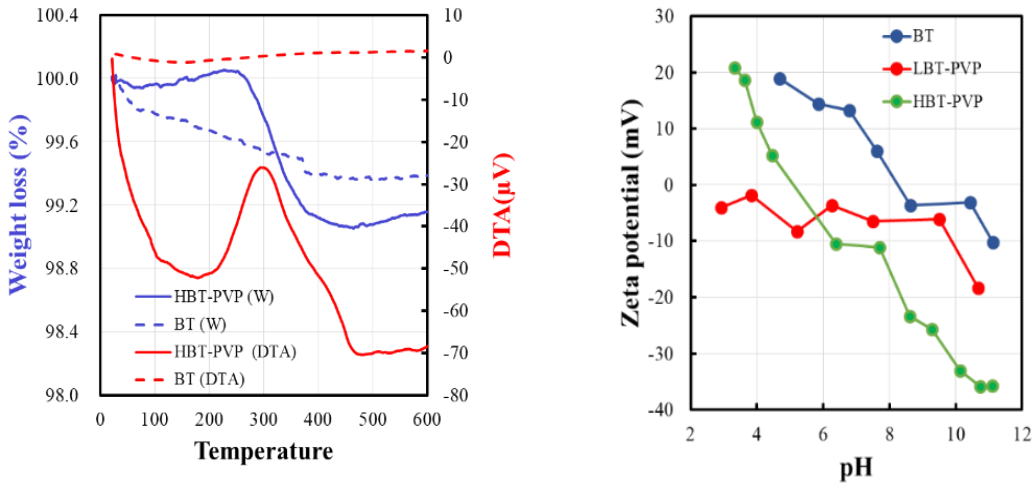

(**a**) (**b**)

Fig.3.3-8 (a) TGDTA of the BT prepared with and without PVP. (b) Relationship between zeta potential and pH. The LBT-PVP is that prepared by low temperature synthesis and the HBT-PVP is that prepared by hydrothermal method.

Fig. 3.3-8(a) shows the TGDTA of the BT prepared with and without PVP. The HBT-PVP prepared with PVP has a weight loss about 1wt% from 200 to 700 ºC and large exothermic peak around 200- 400 ºC, but the BT prepared without PVP does no observe weight loss and exothermic peak, indicating that the dispersant does not exists in the BT surface. Fig. 3.3-8(b) shows the relationship between the zeta potential and pH of BT, LBT–PVP, and HBT–PVP suspension. The LBT-PVP were prepared at low temperature synthesis under atmosphere and the HBT-PVP were prepared by hydrothermal method. Comparing with commercial BT without PVP coating, the zeta potential is from 20 to 40 mV as the pH is around 3-11, and the zeta potential of the LBT-PVP around - 4- -10 mV with pH increasing from3 to 10 which demonstrate that the zeta potential is independence pH. As the Li et al., [25] reported that the dispersion is via the PVP steric effect of LBT-PVP, On the other hand, it can be observe that zeta potential of the HBT-PVP decreases from 20 to -40 mV with pH increasing from 3 to 12. The zeta potential of HBT-PVP aqueous suspension is about -25.6 mV before the HBT-PVP suspension was adjusted that sufficiently maintain the high dispersion. It was close to –30 mV, at which the suspension was physically stable [26]. These demonstrate that the mono-dispersion of the HBT–PVP is realized by electrostatic repulsion. It different from the LBT–PVP as the section 2.4.2 describe that the high dispersion is achieved by the PVP steric effect. It is speculated that

the PVP structure has been changed.

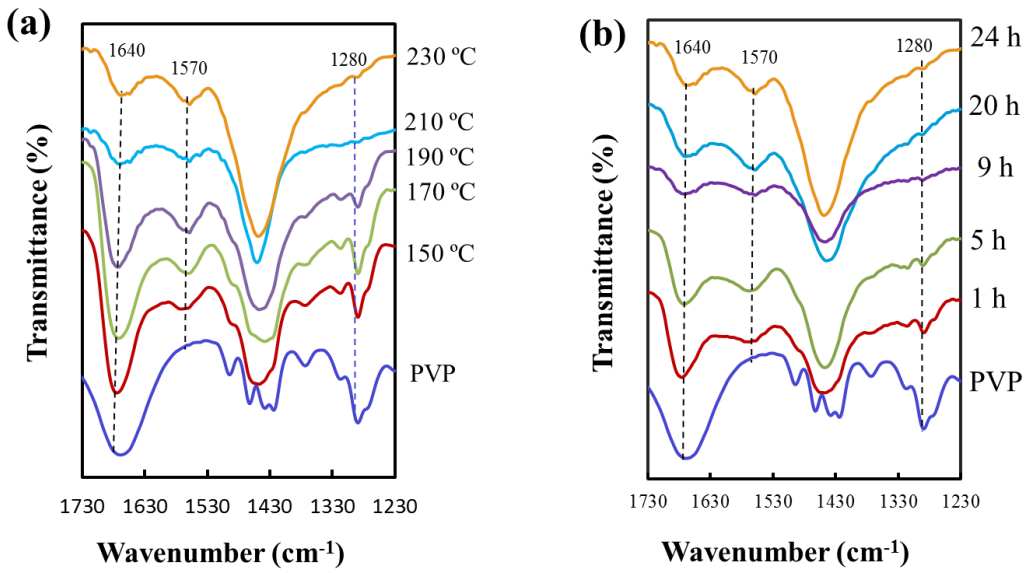

Fig. 3. 3-9 FT-IR spectrum of PVP and HBT–PVPs prepared in different reaction temperature (a) and time (b).

PVP is an amphiphilic dispersant. In our previous study it has been reported that the high dispersion of LBT–PVP prepared in low temperature synthesis is realized by PVP steric effect that PVP adsorbed on the surface. Izu et al., [27]and Ito et al., [28] have reported that the PVP cross–linking was observed on the surface of CeO_2 nanoparticles prepared under atmospheric pressure, and the pyrrolindone ring of PVP opened from the band of N-C=O in acidic solution. But we know that the dispersion of the HBT–PVP that prepared by hydrothermal is realized by electrostatic repulsion. Therefore, it is necessary

to investigate the molecular structure of PVP in order to distinguish the different mechanism of HBT-PVP prepared by hydrothermal method. Fig. 3. 3-9 shows the FT-IR spectrum of PVP and HBT–PVPs prepared in different reaction temperature (a) and time (b). Peaks of the PVP at 1640 cm^{-1} is attributed to symmetric C=O stretching, and 1280 cm^{-1} corresponds to ring (CH_2) wag + (CN) stretching [29]. The peak of C=O does not change with reaction temperature and time, but the corresponding peak of pyrrolindone at 1280cm^{-1} is decreased with temperature and time increasing. And a new peak at 1570 cm^{-1} is observed that maybe assigned to N-H bond [30], which increases with temperature and time increasing. So it concludes that PVP decomposes with reaction temperature and time increasing, and contributes to high dispersion as an ionic dispersant.

3.3.4. Effect of PVP concentration on particle BT growth and dispersion

The high dispersion of HBT-PVP is maintained via electrostatic repulsion, although PVP decomposes in hydrothermal process as the above section described. So the effect of PVP concentration is also important fact for HBT-PVP.

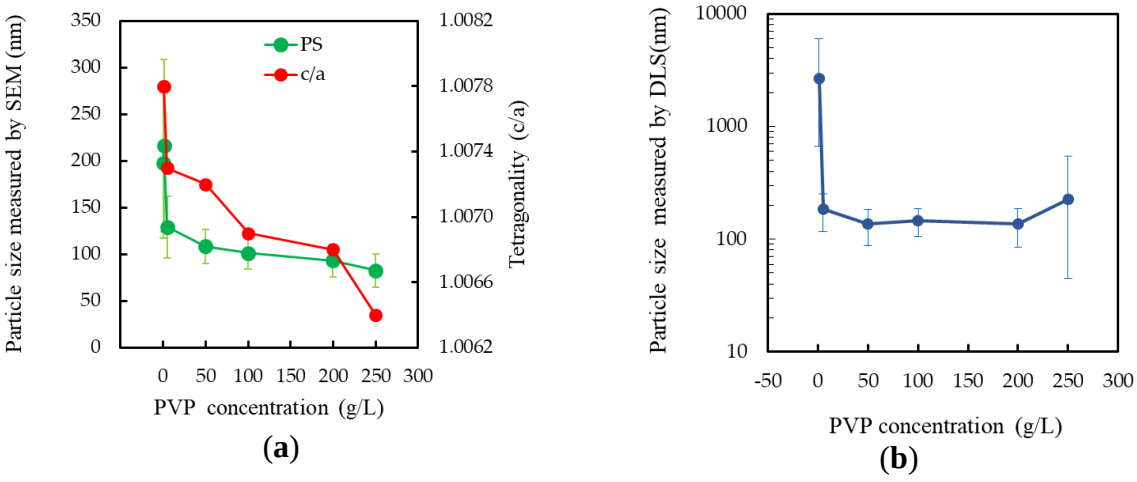

Fig. 3.3-10 Effect of PVP concentration on HBT-PVP (a) particle size measured by SEM and tetragonality (b) particle size measured by DLS.

Fig.3.3-10 (a) shows the effect of PVP concentration on the particle size measured by SEM and tetragonality. The particle size and tetragonality of HBT-PVP decreases with PVP concentration increasing and leads to lower tetragonality of HBT-PVP. And it indicates that PVP inhabits HBT-PVP particle growth, and results the tetragonality reduction. Fig.3.3-10 (b) shows the effect of PVP concentration on dispersion evaluated by particle size measured by DLS. The high dispersion of HBT-PVP is maintained as the PVP concentration is around 5-250 g/L. It indicates that small quantity of PVP can be maintain the high dispersion of HBT-PVP. The amount of PVP increases, the error bar of particle size measured by DLS is increasing. It means that the dispersion slightly becomes

worse, because the particle size of HBT-PVP powder decreases with PVP concentration increasing.

3.4 Conclusion

Highly disperse tetragonal BT nanoparticles can be prepared in one step by hydrothermal synthesis method via the PVP-assisted. In particular, almost mono-disperse HBT–PVP nanoparticles with size of 108 nm and tetragonality factor (c/a) of 1.0072 were easily synthesize via controlling temperature, time and different Ti source. The reaction temperature and time do not significantly affect the growth of HBT–PVP particles, but also affect the dispersant chemical structure. The high dispersion of HBT–PVP is maintained although PVP decompose with reaction temperature and time. The dispersion mechanisms of BT–PVP varied with the synthetic method. The dispersion of LBT–PVP prepared in low temperature directly synthesis is via steric effect of PVP, and the dispersion of HBT–PVP prepared by hydrothermal method is via electrostatic repulsion of decomposed PVP. In addition, the produced HBT–PVP nanoparticles prepared by hydrothermal method exhibited a core-shell structure, as indicated by the results of TEM studies. And at the same time the HBT-PVP prepared by TiO_2 can be obtain higher tetragonality particle than by $TiCl_4$ for the different particle growth mechanism.

3.5 References

[1] M. Stachiotti, *Appl. Phys. Lett.* 2004, 84, 251–253.

[2] J. Varghese, R. W. Whatomore and J.D. Holmes, *J. Mater. Chem*. 2013, 1, 2618–2638.

[3] Y W. S. Yun, J.J. Urban, Q. Gu and H.Park. *Nano. Lett.* 2002, 2, 447–450.

[4] D. Berlincourt and H. Jaffe, *Phys. Rev.* 1958, 111, 143–148.

[5] N. Novak, R Pirc and Z. Kutnjak, *Phys. Rev. B.* 2013, 87, 104102.

[6] S. Wada, K. Yamato, P. Pulpan, N. Kumada, B.-Y. Lee, T. Iijima, C. Moriyoshi and Y.Kuroiwa, *J. Appl. Phys.* 2010,108, 094114.

[7] P. K. Dutta and J. R. Gregg, *Chem. Mater.* 1992, 4, 843–846.

[8] J. Q. Ecker, C. C. Hung-Houston, B. I. Gersten, M. M. Lencka, and R. Riman, *J. Am. Ceram. Soc.* 1996, 79, 2929–2939.

[9] A. Testino, M. T. Buscaglia, V. Biscaglia, M. Viviani, C. Bottino, and P. Nanni, *Chem. Mater.* 2004, 16, 1536–1543.

[10] M. Ryu, T. Suzuki, K. Kobayashi, T. Sakashita, and Y. Mizuno, *Jpn. J .Appl. Phys*. 2010, 49, 061101.

[11] J. Adam, G. Klein and T. Lehnert, *J. Am. Ceram. Soc.* 2013, 96, 2987–2993.

[12] S. Kwon, B. Park, K. Choi, E. Choi, S. Nam, J. Kim, J. Kim, *J. Eur. Ceram. Soc.* 2006, 26, 1401–1404.

[13] A. habbib, N. Stelzer, P. Angerer and R. Haubner, *Bull. Mater. Sci*. 2011, 34, 19–23.

[14] Eckert, J.O., Jr.; Hung-Houston, C.C.; Gersten, B.L.; Lencka, M.M.; Riman, R.E, *J. Am. Ceram. Soc.* 1996, 79, 2929–2939.

[15] Lee, J.J.; Park, K.J.; Hur, K.H.; Yi, S.C.; Koo, S.M, *J. Am. Ceram. Soc.* 2006, 89, 3299–3301.

[16] P.K. Dutta, R. Asiaie, S.A. Akbar, W. Zhu, *Chem. Mater.* 1994, 6, 1542−1548.

[17] M. Wu, R. Xu, S.H. Feng, L. Li, D. Chen, Y.J. Luo, *J. Mater. Sci*. 1996, 31, 6201−6205.

[18] C.T. Xia, E.W. Shi, W.E. Zhong, J.K. Guo, *Soc.*1995,15, 1171−1176.

[19] Uchino K, Sadanaga E, Hirose T, *J. Am. Ceram. Soc.* 1989, 72, 1555−1558.

[20] T. Hoshina, T. Tsurumi, *J. Ceram. Soc. Jpn.* 2013, 121, 156−161.

[21] F. Maxim, I. Poenaru, F. Teodorescu, *J. Inorg. Chem*. 2014, 30, 5160−5167.

[22] Wada, S.; Nozawa, A.; Ohno, M.; Kakemoto, H.; Tsurumi, T.; Kameshima, Y.; Ohba, Y, J. Mater. Sci., 2009, 44, 5161–5166.

[23] Joung, M-R.; Kim, J-S.; Sing, M.; Choi, J-H.; Nahm, S.; Choi, C-H.; Sung, T-H, J. Alloys. Compd., 2011, 509, 9089-9092.

[24] Han, J-M.; Joung, M-R.; Kim, J-S.; Lee, Y-S.; Nahm, S.; Choi, Y-K.; et al., J. Am. Ceram. Soc., 2014, 97, 346–349.

[25] J. Li, K. Inukai, Y.Takahashi, A. Tsuruta, W. Shin, J. Asian. Ceram. Soc., 5(2017) 216–225.

[26] Müller RH. Zetapotential und Partikelladung in der Laborpraxis. Stuttgart: Wissenschaftliche Verlagsgesellschaft; 1996.

[27] N. Izu, T. Uchida, I. Matsubara, T. Itoh, W. Shin, M. Nishibori, Mater. Res. Bull. 46 (2011) 1168–1176.

[28] T. Itoh, N. Izu, I. Matsubara, W. Shin, M. Nishibori, *Chem. Lett.* 2008, 37, 1116–1117.

[29] A. Kedia, PS. Kumar, *J. Phys. Chem. C.* 2012, 116, 23721–237728.

[30] K. Shiba, T. Sugiyama, T. Takei and G. Yoshikawa, *Chem. Commun.* 2015, 51, 15854–15857.

4. Thin Film prepared by BT-PVP

4.1 Introduction

BT is not only used as ferroelectric and piezoelectric material, but also expected in erasable image devices and optical application for its high refractive index [1. 2]. In recent years with miniaturization of devices and thin film, the demand for nano sized BT has increased. In order to meet the need of market, many approaches of thin film prepared have been greatly developed. Typical methods are mainly chemical solution deposition by the sol-gel process [3] or physical depositions by sputtering [4], pulsed laser ablation [5], and chemical vapor deposition [6]. The sol-gel process is the most popular for it can be easy to obtain large-area thin films with good homogeneity and smooth surface at low temperatures. To obtain the high quality film, the sol-gel solution is coated on substrate by dip coating [7, 8] or spin coating [9, 10], then it is treated by high-temperature to obtain BT crystal.

The aggregation of nanoparticles is a serious problem with the particle size decreasing. It will be cause defect in the thin film, and reduce the performance of device. In order to solve this problem, two types high dispersion nanoparticle BT-PVP were prepared by low temperature synthesis (LTS) and hydrothermal method (HT) with polyvinylpyrrolidone

(PVP) assisted as the chapter.2 and chapter.3 described.

In this charper BT-PVP thin film were prepared with these high dispersion nanoparticles suspension by bar coating easily and quickly [11] without further high temperature treatment. And the commercial BT film was also prepared as a comparison. The morphology, thickness, roughness of these thin films were evaluated to understand the dispersant PVP contribute to dense smooth the thin film prepared.

4.2 Experiment

The $BaTiO_3$ powder is referred to LBT-PVP and HBT-PVP prepared by LTS and HT respectively. The LBT-PVP nanoparticle were prepared by LTS as the charper.2 described. The HBT-PVP nanoparticle were prepared by HT as charper.3 described. And the nanoparticle $BaTiO_3$ powder was purchased from Sigma-Aldrich, USA.

The suspension of LBT-PVP, HBT-PVP and BT in EtOH solution with different concentration around 1-10 wt% were used as coating agent. The thin film were deposited by bar coating in manual on polyethylene terephthalate (PET; Toray, Tokyo, Japan) and Si substrates using a bar coater (Matsuo Sangyo Co. LTD., Japan) with a coating speed of about 1.3 m/min. The standard bar RSD20 which its diameter is 6 mm and diameter of winding is 0.5 mm was used to control the thickness of the films. After coating the film

were dry around 80 ºC for 5min.

The particle properties of BT-PVP were evaluated by XRD, DLS, SEM and FT-IR as Chapter. 2 and Chapter. 3 described. The surface roughness of the film was measured using a surface profilometer (P-17 stylus profiler, KLA-Tencor Co., USA), which includes the evaluation of film thickness. Transmittance of light by BT-PVP film on PET were characterized using JASCO V-670 ultraviolet–visible (UV–Vis.) spectrophotometer.

4.3 Results and discussion

4.3.1 Difference BT-PVPs synthesis

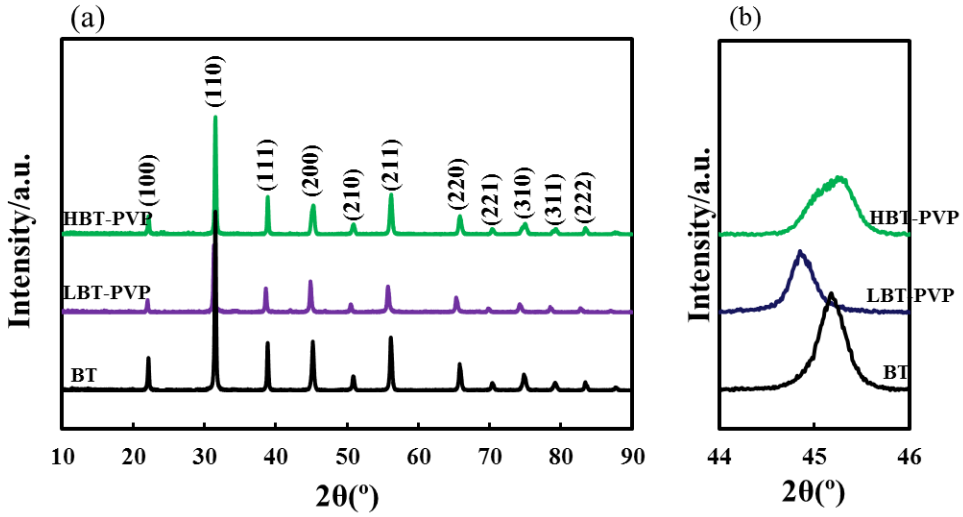

Fig. 4.3-1 XRD pattern of BT, LBT-PVP and HBT-PVP (a) and magnification from 44 to 46º (b).

In this section the BT, LBT-PVP and HBT-PVP were used. Fig.4.3-1 shows their XRD patterns. The crystal phase of BT and LBT-PVP is cubic and LHT-PVP is tetragonal for their XRD patterns is good agreement to the PDF card NO: 01-079-2263 and 01-079-2264 respectively. The characteristic of tetragonal BT is the splitting of (200) plan. Although splitting (200) plan of LHT-PVP is not observed, but it is broader than BT and LBT-PVP. The tetragonality of BT, LBT-PVP and HBT-PVP is 1.0008, 1.0005 and 1.0058 respectively, which calculated by Guassian fitting the (200) plan. In the other words the crystal phase can be controlled in synthesis stage.

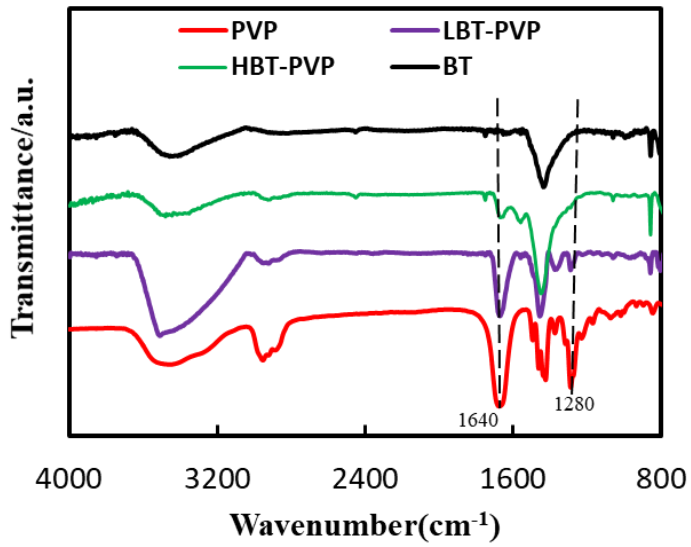

Fig. 4.3-2 FT-IR spectra of BT, LBT-PVP, HBT-PVP and PVP

The surface morphology of BT-PVP particle was evaluated by FT-IR as Fig.4.3-2 showing. The peak of 1640 cm^{-1} is attributed to symmetric C=O stretching and 1280cm^{-1}

corresponds to ring (CH2) wag +(CN) stretching of PVP rings [12]. The peak of 1640 cm^{-1} and 1280 cm^{-1} can be observed for the LBT-PVP, but the peak of 1280 cm^{-1} could not be observed for HBT-PVP. It indicates that PVP does not decompose in LTS but decompose in HT. In the other words, the surface morphology of LBT-PVP and HBT-PVP are difference. As the Chapter.2.3 describe, the high dispersion of LBT-PVP and HBT-PVP via the steric effect of PVP and electric repulse of decomposed PVP in the aqueous solution.

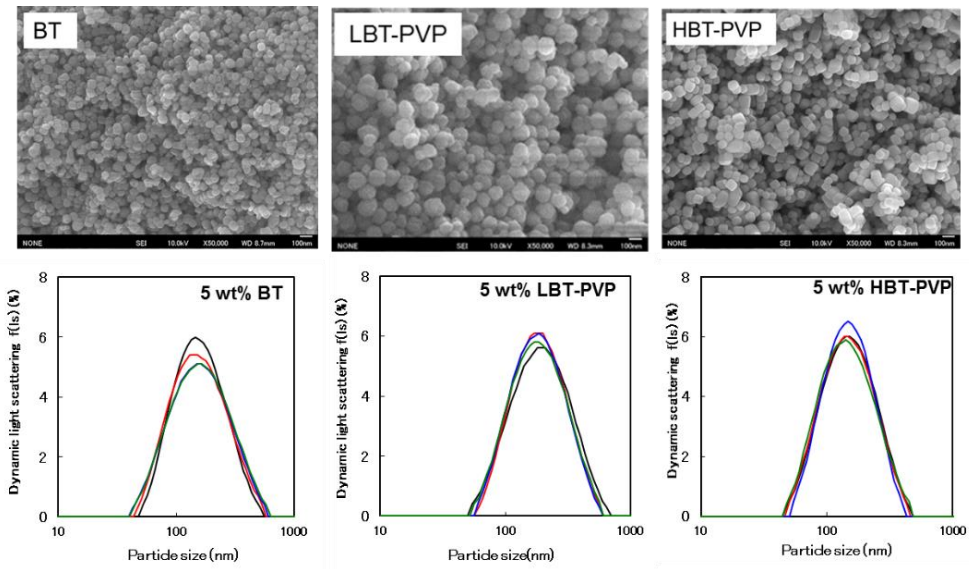

Fig. 4.3-3 SEM images of BT, LBT-PVP and HBT-PVP particle (top), DLS pattern of 5 wt% BT, LBT-PVP and HBT-PVP in EtOH (bottom).

Fig. 4.3-3 is the SEM images of BT, LBT-PVP and HBT-PVP particle. The particle size is 80, 128, 106 nm respectively. These powder were dispersed into EtOH. The particle

size in EtOH is 141, 164 and 131nm measured by DLS. The particle size is very close measured by SEM and DLS respectively. These demonstrate that BT, LBT-PVP and HBT-PVP are monodispersion in EtOH suspension as Fig.4.3-3 (bottom) showing. The comercial BT has a high dispersion in EtOH as BT-PVP because EtOH (25.3) have a small relative permittivity, and lead to a high zeta potential in EtOH solution according to Helmholtz-Smoluchowski formula. The properties of these particles were summarized in Table 4.3-1.

Table. 4.3-1 Properties of BT, LBT-PVP and HBT-PVP.

Particles	Particle size (nm)				Tetragonality (c/a)
	SEM	CV(%)	DLS	CV(%)	
BT	81.0	20.1	141	55.2	1.0008
LBT-PVP	128	16.6	164	48.2	1.0005
HBT-PVP	106	20.7	131	47.2	1.0058

4.3.2 Preparation of thin film

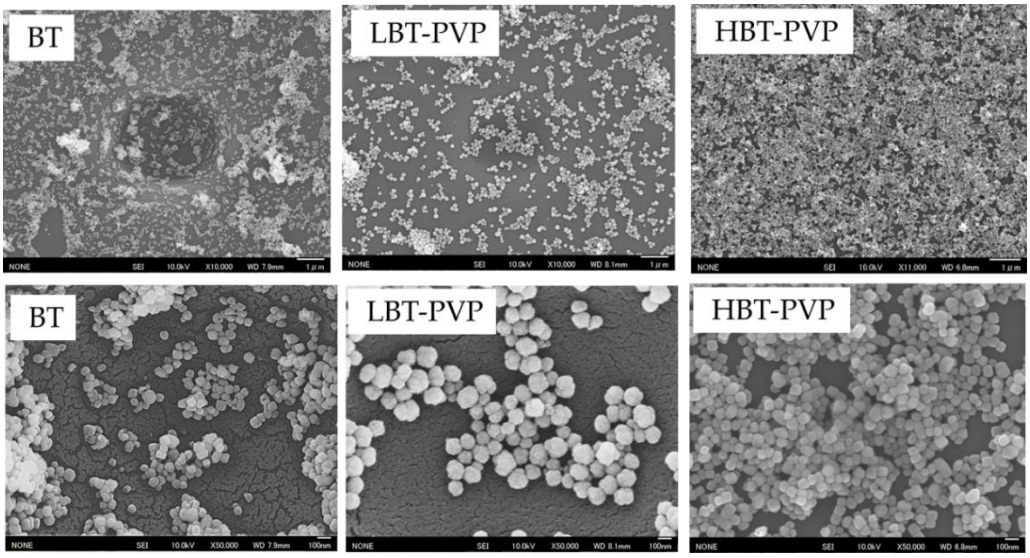

Fig. 4.3-4 SEM mages of thin film prepared by 1 wt% of BT, LBT-PVP and HBT-PVP

in EtOH. The substrate is PET film. The upward is reduced, and the downward is enlarged images.

The particles of BT. LBT-PVP, HBT-PVP have a characteristic of monodispersion in EtOH solution. These particles were dispersed into EtOH solution which used as coating agent with different particle content. The film were coated on PET and Si substrate by simple bar coating in manual. The coating speed is about 1.3 m/min. Fig. 4.3-4 shows the SEM images of thin film coated on PET prepared by 1 wt% content of particle in coating agent. It could be seen that the packing density of the film prepare by 1wt% coting agent is very low, but it can be seen that the BT film has much large aggregate, but the particles disperse relatively evenly on the PET film for LBT-PVP and HBT-PVP. It may be due to dispersant that coated on the surface BT, which prevents aggregate from BT nanoparticles as EtOH solution evaporate during film drying. The particle density of HBT-PVP film is relatively higher than LBT-PVP film could also be observed in Fig. 4.3-4 (down), in the other wards the coverage of HBT-PVP particle on PET substrate is higher than LB-PVP. It maybe relate to the dispersion mechanism difference of decomposed PVP and PVP that coating on the BT surface. The electrostatic repulse is more effective than steric effect to reach equilibrium with capillary force and van der walls force inter-particle assembly in

short-range of particles as the EtOH is dried.

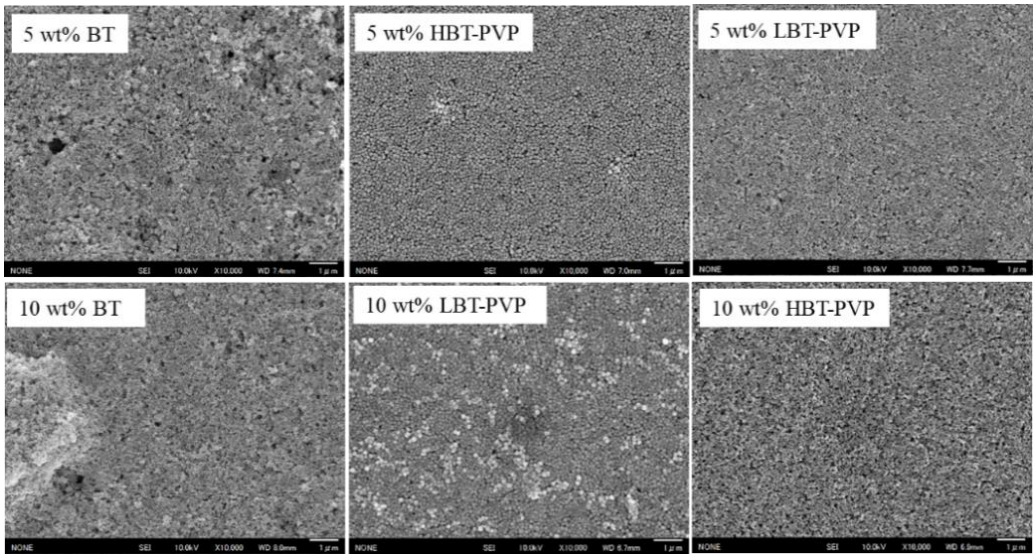

Fig. 4.3-5 SEM mages of thin film prepared by 5 and 10 wt% of BT, LBT-PVP and HBT-PVP in EtOH. The substrate is PET film.

Fig. 4.3-5 shows the morphology of thin film prepared by 5, and 10 wt% BT, LBT-PVP and HBT-PVP with difference content. It can be seen that the thin film become dense and smooth with powder content increasing. Although As the particle content increases to 5 wt%, the films become dense but many large holes can be observed for BT film, on the contrary the films of LBT-PVP and HBT-PVP are very smooth and dense. And then the particle content increases to 10 wt%, the HBT-PVP film becomes denser and smoother, but several aggregates could be observed on LBT-PVP film. It also demonstrates the importance and difference of PVP and decomposed PVP adsorbed on the surface of

nanoparticle.

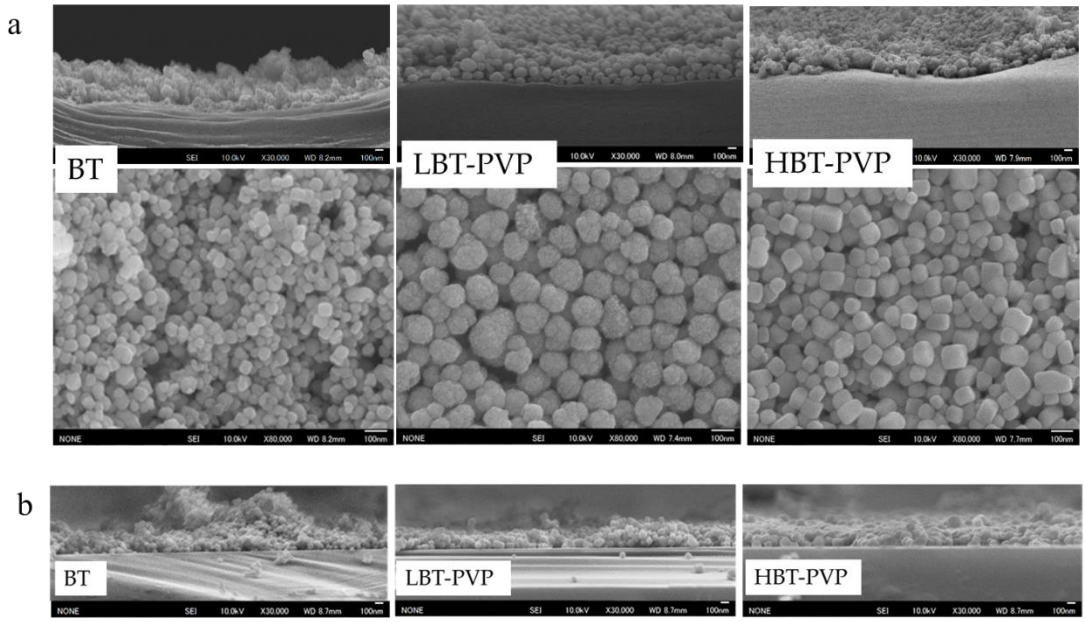

Fig. 4.3-6 SEM images of thin films prepared by 5 wt% BT, LBT-PVP and HBT-PVP in EtOH solution on PET (a) and Si substrate (b). Upside cross section is on PET, downside cross section is on Si substrate.

The thickness is around 250-300 nm from the cross section (Fig. 4.3-6(up)). The BT film is very rough. The interface of PET and film is distorting for the PET is very flexible.

The particles aggregate and much defect can be observed in BT film (Fig. 4.3-6(middle)), on the contrary, the particle is neatly and densely arranged for in BT-PVP films. It is well known that the BT thin film coated on Si wafer is expected to use for microelectronic device. In addition, in order to accurately the film properties such as thickness, roughness, The films were also prepared on Si substrate as the same condition on PET which the inter face is straight as Fig. 4.3-6(b) showing. The thickness of BT, LBT-PVP, HBT-PVP

film are 209, 292, and 293 nm, respectively.

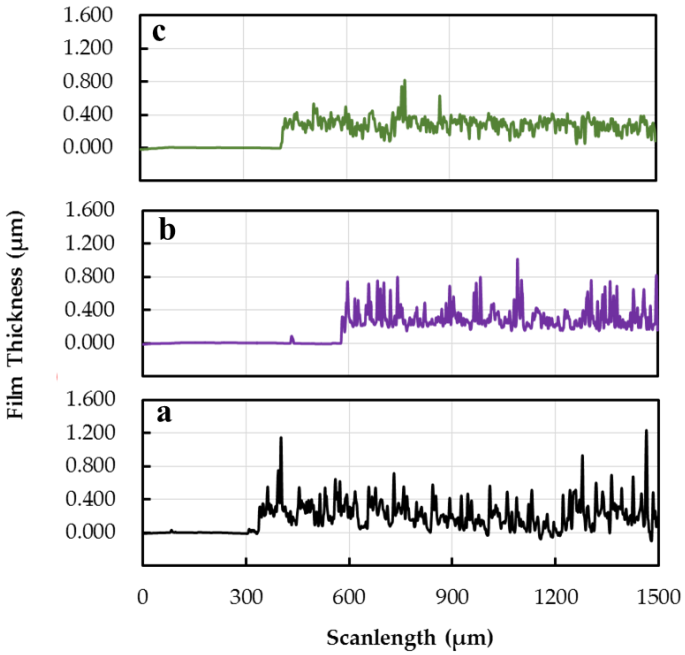

Fig. 4.3-7 Surface profiles of thin films coated on Si substrates measured by stylus profiler. (a)BT (b) LBT-PVP (c) HBT-PVP.

Furthermore the thickness and roughness were measured by a surface profiler. Fig. 4.3-7 shows the surface profiles of thin films coated on Si substrates measured by stylus profiler. . The film thickness is 226, 308 and 283 nm for BT LBT-PVP and HBT-PVP respectively, which is close to that measured by SEM images. And the roughness is 104.6, 91.6, and 56.1 nm. It is agree to the SEM observation that the surface of BT-PVP films are smoother than BT film. Table.4.3-2 summarized these results in detail.

Table.4.3-2 results of film thickness and roughness coated on PET and Si substrate

Particles	Film Thickness (nm)			Ra* (nm)
	PET	Si		
	SEM	SEM	profiler	
BT	268.2	209.4	226.2	104.6
LBT-PVP	307.9	292.1	308.4	91.6
HBT-PVP	266.8	293.2	283.1	56.1

It can be also known that the HBT-PVP film is smoother than LBT-PVP film for the roughness is 56.1, and 91.6 nm for HBT-PVP, and LBT-PVP film, respectively. It is thought that the decomposed PVP adsorbed on the BT surface is more effective to inhabit the nanoparticle aggregate than PVP adsorbed on BT during EtOH evaporation. In the other words that the electronic repulse of decomposed PVP is more effective to prevent the nanoparticle aggregate than steric effect of PVP in the film drying process.

At the same time it also can be seen that the face-to-face particle ordering in HBT-PVP film as Fig. 4.3-5a shown. This array formed in drying process of film reduces the film roughness. Although nanocube BT assembly thin film which is smooth ,dense and less than 1μm can be prepared by sol-gel method [8, 9], but it requires a long time, and the film is limited to cubic BT. In order to improve the film performance, it has been to heat above 1100°C [10]. In our study the self-assembling process can be simply form in the EtOH evaporation and BT crystalline phase can be controlled in synthesis stage.

The BT-PVP film is very smooth due to the PVP dispersant coated on the BT surface,

with PVP or decomposed PVP, which prevents particle aggregation, and uniform evaporation of EtOH. So it is very important for the formation of a smooth film. The BT-PVP film on a PET substrate demonstrated in this report has the significant advantage of room-temperature coating without thermal treatment. Although several micron thicknesses BT film could be formed by screen print with BT paste, but the film is very coarse and has many defects [13].

4.4 Conclusion

High dispersion BT nanoparticle were synthesized by low temperature directly synthesis and hydrothermal method with PVP assistance at 80ºC and 230ºC, respectively. LBT-PVP and HBT-PVP were applied to prepare BT thin film by bar coating with their EtOH suspension in different concentration on PET and Si substrate. And commercial BT film was also prepared as comparison. Bar coating is very simple and quick to form thin film. The film thickness can be controlled by choosing a wire diameter and concentration of coating agent.

The thickness of BT, LBT-PVP, and HBT-PVP film coated on Si substrate are 226, 308, and 283 nm, and their surface roughness were104.6, 91.6, and 56.1 nm respectively. PVP plays an important role in forming smooth and dense BT thin film, which can be prevent

nanoparticle aggregate in EtOH evaporation.

4.5 References

[1] Y. Yang, J. Shi, W. Huang, S. Dai, L. Wang, *J. Mater. Sci*. 2003, 38, 1248.

[2] Z.G. Hu, G.S. Wang, Z.M. Huang, J.H. Chu, *J. Phys. Chem. Solids.* 2003, 64, 2450.

[3] H. Kozuka, *Jpn. J. Ceram. Soc*. 2003, 111, 624–632 .

[4] P. Bhattacharya, T. Komeda, D. Park and Y. Nishioka, *Jpn. J. Appl. Phys.* 1993,32, 4103.

[5] S. G. Yoon, J. Lee and A. Safari, *Integrated Ferroelectrics A*, 1995, 7, 329–339.

[6] D. Tahan, A. Safari and L. C. Klin, *J. Am. Ceram. Soc. C*, 1996, 79, 1593.

[7] H. Kozuka and M. Kajimura, *J. Am. Ceram. Soc.* 2000, 83(5), 1056–1062.

[8] K. Mimura and K. Kato, *Jpn. J. Appl. Phys.*2013, 52(9), 09KC061-5.

[9] K. Mimura, T. Naka, T. Shimura and W. Sakamoto, and T. Yogo, *Thin Solid Films*. 2008, 516, 8408–8413.

[10] B. Lee and Jianping, *Thin Solid Films*. 2001, 388, 107–113.

[11] T. Itoh, T. Uchida, N. Izu and W. Shin, *Materials.* 2017, 10, 710–723.

[12] A. Kedia, PS. Kumar, *J. Phys .Chem C.* 2012, 116, 23721-237728.

[13] B. D. Stojanovica, C. R. Foschinic, V. Z. Pejovicd, V. B. Pavlovice and J. A. Varelaa,

J. Eur. Ceram. Soc. 2004, 24, 1467–1471.

5. Summary

In this study, the high dispersion nanoparticle of BT-PVP was synthesized by low temperature synthesis, and hydrothermal method. The reaction factors such as reaction temperature, reaction time, PVP concentration, molecular weight of PVP were investigated. The high dispersion of BT-PVP nanoparticle can be synthesized by systemic controlling this factor. The difference of BT-PVPs prepared by these two methods was compared in particle growth and dispersion mechanism.

In chapter 2, the LBT-PVP was synthesized in low temperature under atmospheric pressure. The reaction factors of reaction temperature, time, concentration of raw material, KOH, and PVP, and PVP molecular weight were investigated. The particle growth of LBT-PVP was evaluated by XRD and TEM. The particle is a polycrystal consisted several different orientation cubic crystals. The concentration of KOH does not only affect the particle growth, but also affect the dispersion of BT-PVP. The PVP is adsorbed on the both the inside and the surface of the particles. The amount of PVP adsorbed on the surface was related to the dispersity of LBT–PVP. The high dispersion was realized by PVP steric effect. There is optimum synthesis condition area for high dispersion by systemic controlling these factors as the Fig. 2.5-1 showing. The almost mono-dispersion

LBT-PVP about 114 nm could be prepared by in condition of Ti/Ba = 0.2 M: 0.3 M, [KOH] = 1.4 M, [PVP] =100 g/L at 80 ºC.

In chapter 3, the HBT-PVP was prepared by hydrothermal. The reaction factor of reaction temperature and time were investigated with $TiCl_4$ as Ti source. The particles morphology changes from spherical, torus-like shape, round corner cube to sharp cube , and the crystal phase of HBT-PVP is from cubic to tetragonal with temperature and time increasing. Although PVP decomposed in this high temperature and high pressure, but the high dispersion could be maintained by the electrostatic repulsion. It is different from the dispersion mechanism of PVP in low temperature atmosphere which is via steric effect. Mono-dispersion HBT-PVP obtained from 190 ºC for 24h. A the same time, in order to obtain high tetragonality HBT-PVP, TiO_2 was also use as Ti source for its different reaction mechanism to $TiCl_4$. The results demonstrate that higher HBT-PVP could be obtained by TiO_2 than by $TiCl_4$. Furthermore the effect of PVP concentration on HBT-PVP particle growth and dispersion was also investigated. The PVP is not effect dispersion of HBT-PVP but also effect the particle growth.

Each of these two methods has advantages and it can be used in conjunction with the purpose. Large amount of highly dispersive cubic BT-PVP could be obtained by the low temperature synthesis atmospheric method. Highly dispersive tetragonal BT-PVP could

be obtained by hydrothermal method.

In chapter 4, the particles LBT-PVP and HBT-PVP which prepared by LTD and HT respectively were used to prepared thin film on PET and Si substrate by bar coating. The BT-PVP film is very smoother and denser than BT film that without PVP coating. The role of PVP that coated on BT is that prevents the nanoparticle aggregate, and evenly evaporation of EtOH during thin film drying. The thin film can be simply prepared by bar coating, and unnecessary further high temperature treatment. The phase of BT can be controlled during synthesis.

6. List of publication

Publishes in Journals

1. Jinhui Li, Woosuck Shin, Koji Inukai, Yosukei Takahashi, Synthesis and size control of monodispersed $BaTiO_3$–PVP nanoparticles, Journal of Asian Ceramic Societies, 4, 394-402 (2016)
2. Jinhui Li, Woosuck Shin, Akira Tsuruta, Koji Inukai, Yosukei Takahashi, Effect of PVP on the synthesis of high-dispersion core–shell barium-titanate–polyvinylpyrrolidone nanoparticles, Journal of Asian Ceramic Societies, 5, 216-225 (2017)
3. Jinhui Li, Woosuck Shin, Akira Tsuruta, Koji Inukai, Yosukei Takahashi, Synthesis of highly disperse tetragonal $BaTiO_3$ nanoparticles with core-shell by a hydrothermal method, Journal of Asian Ceramic Societies, 5, 444–451 (2017).
4. Jinhui Li, Koji Inukai, Akira Tsuruta, Yosukei Takahashi, Woosuck Shin, Formation mechanism and dispersion of pseudo-tetragonal $BaTiO_3$-PVP nanoparticles from different titanium precursors: $TiCl_4$ and TiO_2, Materials. 11, (2018) 51.
5. Jinhui Li, Koji Inukai, Akira Tsuruta, Yosukei Takahashi, Woosuck Shin, Thin film Coating with highly dispersible barium titanate- polyvinylpyrrolidone nanoparticles,

(2018) Materials. 11, (2018) 712.

Presentation in conferences

International conference

1. Jinhui Li, Woosuck Shin, Koji Inukai, Yosukei Takahashi, Dispersibility and formation mechanism of BaTiO3 nanoparticles in aqueous solution ,The 11th Pacific Rim Conference on Ceramic Societies August30-September4, 2015, Jeju, Korea, Oral.
2. Jinhui Li, Woosuck Shin, Akira Tsuruta, Koji Inukai, Yosukei Takahashi, Synthesis of high-dispersion BaTiO3-PVP nanoparticles by hydrothermal method. The 8th International Conference on Electroceramics, May 28-31, 2017, Nagoya Japan, Poster.

Domestic conference

1. Jinhui Li, Woosuck Shin, Koji Inukai, Yosukei Takahashi, Annual Meeting of The Ceramic Society of Japan (2016 年年会) Mar. 2016, Tokyo, Japan, Oral.
2. Jinhui Li, Woosuck Shin, Akira Tsuruta, Koji Inukai, Yosukei Takahashi, 29th Fall Meeting of The Ceramic Society of Japan (第 29 回秋季シンポジウム) Sep 19～21 2016, Hiroshima, Japan, Poster.
3. Jinhui Li, Woosuck Shin, Akira Tsuruta, Koji Inukai, Yosukei Takahashi, 30th Fall

Meeting of The Ceramic Society of Japan (第 30 回秋季シンポジウム) Sep 19～21 2017, Koubei, Japan, Oral.

7. Acknowledgment

This study is gratefully supported by Professor Woosuck Shin who is the supervisor of this study. I also thank Professor Masanobu Nakayama (Nagoya Institute of Technology), Professor Takashi Shirai (Nagoya Institute of Technology) for their insightful comments and constructive suggestion on this study.

The supported of Noritake Co Limited’s coworkers (Dr. Yosuke Takahasi, Dr. Koji Inukai), and AIST’s reashers (Dr. Akira Tsuruta) are highly acknowledged.

I also thank my husband Yoshihisha Takayasu, and my children Yuta and Toshiki for their warm encouragement and cooperation.

The contents of chapter. 2, 3 amd 4 have been also published in Journal of Asian Ceramic Societies, and Materials (MDIP) listed as Chapter. 6 of Publishes in Journal.